Materials Sciences Corporation

(2)

AD-A226 060

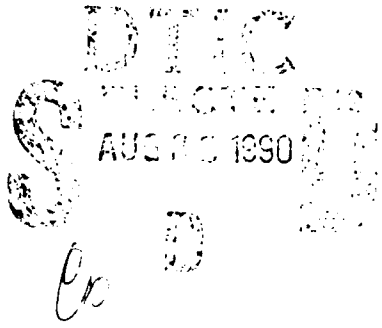

STRUCTURAL DEVELOPMENT OF MICRO-STRUCTURALLY TOUGHENED METAL MATRIX COMPOSITES

Technical Final Report
MSC TFR 2111/8602
July, 1990

Prepared for:

Office of Naval Research
800 North Quincy Street
Arlington, VA 22217-5000

Contract Number N00014-89-C-0211

Phase I Small Business Innovative Research Program
Strategic Defense Initiative Organization
Office of Innovative Science & Technology

90 08 24 025

930 Harvest Drive, Union Meeting Corporate Center, Blue Bell, PA 19422
Tel: 215-542-8400 Fax: 215-542-8401

UNCLASSSIFIED

SECURITY CLASSIFICATION OF THIS PAGE

REPORT DOCUMENTATION PAGE

Form Approved OMB No. 0704-0188

1a REPORT SECURITY CLASSIFICATION: UNCLASSIFIED	1b RESTRICTIVE MARKINGS
2a SECURITY CLASSIFICATION AUTHORITY: N/A	3 DISTRIBUTION/AVAILABILITY OF REPORT
2b DECLASSIFICATION/DOWNGRADING SCHEDULE: N/A	
4 PERFORMING ORGANIZATION REPORT NUMBER(S): MSC TFR 2111/8602	5 MONITORING ORGANIZATION REPORT NUMBER(S)
6a NAME OF PERFORMING ORGANIZATION: Materials Sciences Corporation; 6b OFFICE SYMBOL (If applicable): N/A	7a NAME OF MONITORING ORGANIZATION: Office of Naval Research
6c ADDRESS (City, State, and ZIP Code): 930 Harvest Drive, Suite 300, Blue Bell, PA 19422	7b ADDRESS (City, State, and ZIP Code): Department of the Navy, 800 North Quincy Street, Arlington, VA 22217
8a NAME OF FUNDING/SPONSORING ORGANIZATION: Strategic Defense Initiative Organization; 8b OFFICE SYMBOL (If applicable):	9 PROCUREMENT INSTRUMENT IDENTIFICATION NUMBER: N00014-89-C-0210
8c ADDRESS (City, State, and ZIP Code): The Pentagon, Washington, DC 20301-7100	10 SOURCE OF FUNDING NUMBERS: PROGRAM ELEMENT NO.; PROJECT NO. s405059 srh01/3/30/89 (1131N); TASK NO; WORK UNIT ACCESSION NO.

11 TITLE (Include Security Classification): Structural Development of Micro-Structurally Toughened Metal Matrix Composites

12 PERSONAL AUTHOR(S): Edward C.J. Wung and Kent W. Buesking

13a TYPE OF REPORT	13b TIME COVERED	14 DATE OF REPORT (Year, Month, Day)	15 PAGE COUNT
Final Report	FROM 89SEP01 TO 90JUN30	90JUN30	69

16 SUPPLEMENTARY NOTATION

17 COSATI CODES		
FIELD	GROUP	SUB-GROUP

18 SUBJECT TERMS (Continue on reverse if necessary and identify by block number): Discontinuously Reinforced Metals, Microstructure Toughening Mechanisms, Silicon Carbide/Aluminum, Impact Damage, Structural Applications, Metal Matrix Composites

19 ABSTRACT (Continue on reverse if necessary and identify by block number): This study addressed the development of a new class of discontinuously reinforced metals that possess substantially improved damage tolerance relative to the currently available materials. The novelty is to allow specially designed toughening mechanisms to be operative in the composites. Technical effort of this study focused on developing a fundamental understanding of the toughening mechanisms at the micromechanics level, and identifying possible SDI structural components that can be improved through the use of this material. This goal was achieved by the development of two micromechanical material models. The first model addressed the stress-strain constitutive modeling, and the second model addressed the modeling of fracture toughness of the new composites. Modeling and data correlation studies have suggested several guidelines for material strength design as well as for toughness design. A submarine hull and an aircraft lower longeron were selected as candidate structural components that might be improved through the use of this new material. A preliminary design of the longeron was performed to demonstrate a design methodology for these new composites.

20 DISTRIBUTION/AVAILABILITY OF ABSTRACT	21 ABSTRACT SECURITY CLASSIFICATION
☒ UNCLASSIFIED/UNLIMITED ☐ SAME AS RPT. ☐ DTIC USERS	UNCLASSIFIED
22a NAME OF RESPONSIBLE INDIVIDUAL: Dr. Steven G. Fishman	22b TELEPHONE (Include Area Code): (202) 692-0285; 22c OFFICE SYMBOL: 1131N

DD Form 1473, JUN 86 — Previous editions are obsolete. SECURITY CLASSIFICATION OF THIS PAGE

UNCLASSIFIED

PREFACE

This report presents the results of a study performed under the Strategic Defense Initiative Organization (SDIO), Contract N00014-14-89-C-0210, during the period of September 1, 1989 through June 30, 1990. The program was funded as a Phase I Small Business Innovative Research Contract. The program manager for Materials Sciences Corporation (MSC) was Mr. Kent W. Buesking. The principal investigator for MSC was Dr. Edward C.J. Wung. Mr. Dave Divecha of Naval Surface Weapons Center (NSWC) served as the Technical Monitor for the contract.

Approved by:

Kent W. Buesking

Kent W. Buesking

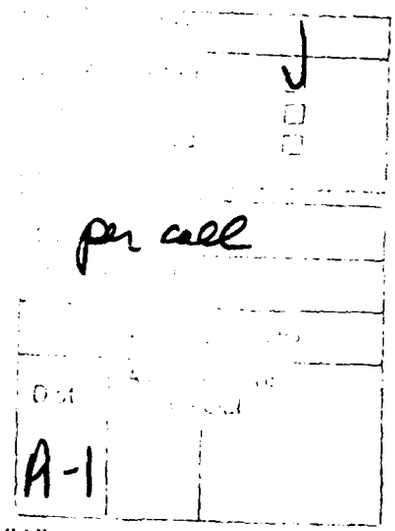

STATEMENT "A" per Dr. Steven Fishman
ONR/Code 1131
TELECON 8/27/90 VG

TABLE OF CONTENTS

Page

INTRODUCTION 1
OBJECTIVES 3
APPROACH 4
Stress - Strain Constitutive Modeling 4
Analysis of Laminated MT Composites 9
Modeling of Impact Damage and Work of Fracture. 10
Structural Component Selection 15
RESULTS 18
Material Properties 18
Stress-Strain Constitutive Relations. 18
Laminated MT Composites 20
Analyses of Impact Damage and Work of Fracture. 21
Optimization of Impact Damage Resistance. 23
Preliminary Component Design 24
CONCLUSIONS AND RECOMMENDATIONS. 27
REFERENCES 29
TABLES 31
FIGURES 36
APPENDIX - Thermoplastic Response of a Homogeneous Solid 62

INTRODUCTION

Discontinuously reinforced metals are a class of composites which have witnessed extensive development over the past several years [1-4]. Most of the research has focused on the development of silicon carbide (SiC) particulate reinforced aluminum alloys, but reinforced magnesium, titanium and nickel based superalloys are also receiving attention. Although the discontinuously reinforced metal matrix composites exhibit some favorable attributes such as the enhanced stiffness and reduced CTE, their one principal drawback is the substantially reduced damage tolerance relative to the matrix material.

A novel fabrication approach that introduced a toughening mechanism into the discontinuously reinforced metals has been developed recently at United Technologies Research Center (UTRC) [5]. A schematic microstructure of such a "microstructurally toughened" (MT) composite is shown in Figure 1. The energy absorption capability of the MT composites is enhanced by the following two mechanisms. First, when cracks encounter interfacial areas between the reinforced and toughening regions, debonding at the interface can result in crack tip blunting. Second, the inherently higher energy absorption capability of the toughening region inhibits crack propagation.

A MT composite consisting of silicon carbide particulate reinforced 6061 aluminum, with either aluminum or titanium tubings as the toughening region material was selected as a model system to evaluate the merits of the toughening approach. Note that the MT composite system with aluminum tubings as the toughening region material has been shown to have a fracture toughness ranging from 5 to 12 ft-lbs, as compared to 0.8 ft-lbs for the particulate reinforced material without toughening mechanism [5].

The primary goal of this study was to support the ongoing development of the MT composites at UTRC through better understanding of the merits of the toughening mechanism at the micromechanics level, and to develop a design methodology for MT composites that can take full advantage of the unique characteristics of these materials. This goal was met by: compiling a design database of MT composite material properties; analyzing the material properties using micromechanical and composite material models to understand the measured material stress-strain behavior and impact damage resistance; reviewing SDI

structural components and requirements to select attractive components, and developing preliminary material and structural designs.

OBJECTIVES

The MT composites developed recently at UTRC have successfully demonstrated that the fracture toughness of the discontinuously reinforced metals can be greatly improved if certain toughening mechanisms can be introduced into the material microstructures [5]. The primary goal of this study was to support the ongoing development of the MT composites through better understanding of the merits of the toughening mechanism at the micromechanics level, and to develop a design methodology for SDI structural applications that can take full advantage of the unique characteristics of MT composites.

The goal was achieved by the development of two micromechanical material models. The first model addresses the stress-strain constitutive modeling of MT composites based upon the material properties and volume fractions of the constituents. No considerations regarding geometric shapes and dimensions of the toughening region were given in this model. The model was used strictly to predict the material stiffness or compliance matrix which was required for stress analysis of structural components made of MT composites.

It was well documented in [5] that while the actual dimensions and shape of the toughening region rarely affected the stress-strain behavior of MT composites, they did influence the ability of the composites to withstand impact damage. Therefore, a second model was developed to address the possibility of predicting the fracture toughness of the MT composites by taking the geometric factors into account.

A submarine hull and an aircraft longeron were identified in this study as possible components that can be improved through the use of MT composites. A preliminary design of the aircraft longeron was performed to demonstrate a design methodology for MT composites.

APPROACH

Evidence in UTRC testing results suggested that the stress-strain behavior and the impact damage absorption capability of the MT composites were governed by different sets of material and geometric variables. Therefore, two micromechanical models were developed to study these two phenomena separately. The stress-strain model was further incorporated into an existing MSC computer code "EPLAM" which was developed earlier by MSC staff for elastoplastic incremental laminate analysis [6]. This revised analysis gives us the ability to deal with laminated MT composites which is expected to be an important step in the future material development. The theoretical basis for the models are discussed in the following sections. A description of the structural component selection is also included.

STRESS-STRAIN CONSTITUTIVE MODELING

From a microstructural standpoint, the MT composites can be treated as continuous fiber reinforced composites, with the reinforced regions being analogous to the fibers (fig. 2). Two existing material models, composite cylinders assemblage model (CCA) [7], and vanishing fiber diameter model (VFD) [8], have been applied successfully to describe elastoplastic behaviors of fiber reinforced metal matrix composites. However, our past modeling experience indicated that CCA model might not be suitable for evaluating MT composite properties. The reason being CCA model always imposes a perfect bonding between constituent phases while MT composite properties are strongly affected by the bonding strength of the interface which could be rather low in practice. Of course, a modified three-phase CCA model with the interface region being the 3rd phase can be constructed [9]. However, the mathematical complexity of this new model is beyond the scope of our current study.

Due to this consideration, VFD model was chosen for the purpose of stress-strain modeling. It should be noted that we also recognized the fact that VFD model always assumes uniform transverse stress distribution in the phases, and this is not suitable for modeling MT composites either. However, the simplicity of the model and the fact that the model generally gives very

accurate prediction in axial stress-strain response make VFD model a desirable choice for initial material modeling.

The existing formulation for VFD model in reference 8 was derived for modeling fibrous composites with elastic fibers embedded in ductile metal matrix, and the materials were exposed to pure mechanical loads. Since the reinforced region of MT composites, which was to be modeled as fibers, could be ductile in general; therefore, analytical effort was required to extend the existing VFD model to account for the presence of ductile fibers. In addition, to analyze MT composites for high temperature applications, the modeling should also include thermal effects. The mathematical formulation of this extended VFD model will be described next.

VFD model assumes the following equilibrium and compatibility equations:

$$d\sigma_{ij} = d\sigma_{ij}^{(f)} = d\sigma_{ij}^{(m)} \quad \text{for } ij \neq 11, \tag{1}$$

$$d\sigma_{11} = c_m d\sigma_{11}^{(m)} + c_f d\sigma_{11}^{(f)}, \tag{2}$$

$$d\epsilon_{ij} = c_m d\epsilon_{ij}^{(m)} + c_f d\epsilon_{ij}^{(f)} \quad \text{for } ij \neq 11, \tag{3}$$

$$d\epsilon_{11} = d\epsilon_{11}^{(f)} = d\epsilon_{11}^{(m)}. \tag{4}$$

$d\sigma_{ij}$ and $d\epsilon_{ij}$ are the uniform stress and strain increments applied to the composite. The index (f) or (m) is used to denote fiber or matrix related quantities. c_f and c_m are volume fractions of the phases such that $c_f + c_m = 1$. Fibers are assumed to be aligned along x_1-direction and x_2 and x_3 are the transverse directions.

As a step beyond the scope of existing VFD model, both fiber and matrix materials are assumed to be elastically isotropic materials which obey Mises yield condition and Ziegler's kinematic hardening rule during plastic deformation [10]. To account for the thermal effects, we further assume that the elastic properties, as well as the yield stresses of both constituents, are temperature dependent. Under such circumstances, the instantaneous thermomechanical responses of the constituents are described by

$$\underset{\sim}{\dot{\epsilon}}^{(r)} = \underset{\sim}{M}^{ef}_{(r)}\, \underset{\sim}{\dot{\sigma}}^{(r)} + \underset{\sim}{\dot{\epsilon}}^{eT}_{(r)} + \underset{\sim}{\dot{\epsilon}}^{p}_{(r)} \tag{5}$$

(r = f for fibers, m for matrix),

where

$$\underset{\sim}{\dot{\epsilon}}^{eT}_{(r)} = (\underset{\sim}{M}^{ef}_{(r)} - \underset{\sim}{M}^{es}_{(r)})\ \underset{\sim}{\sigma}^{s}_{(r)} + \underset{\sim}{\dot{\delta}}^{fs}_{(r)}. \tag{6}$$

$$\underset{\sim}{\dot{\epsilon}}^{P}_{(r)} = \underset{\sim}{M}^{P}_{(r)}\ \underset{\sim}{\dot{\sigma}}_{(r)} + \underset{\sim}{\dot{\epsilon}}^{pT}_{(r)}. \tag{7}$$

The definitions of the variables which appeared in the above equations are:

$$\underset{\sim}{\dot{\epsilon}} = [\dot{\epsilon}_1\ \dot{\epsilon}_2\ \dot{\epsilon}_3\ \dot{\epsilon}_4\ \dot{\epsilon}_5\ \dot{\epsilon}_6]$$
$$= [\dot{\epsilon}_{11}\ \dot{\epsilon}_{22}\ \dot{\gamma}_{12}\ \dot{\epsilon}_{33}\ \dot{\gamma}_{13}\ \dot{\gamma}_{23}],$$

$$\underset{\sim}{\dot{\sigma}} = [\dot{\sigma}_1\ \dot{\sigma}_2\ \dot{\sigma}_3\ \dot{\sigma}_4\ \dot{\sigma}_5\ \dot{\sigma}_6]$$
$$= [\dot{\sigma}_{11}\ \dot{\sigma}_{22}\ \dot{\tau}_{12}\ \dot{\sigma}_{33}\ \dot{\tau}_{13}\ \dot{\tau}_{23}],$$

$\underset{\sim}{M}^{ef}$ = Elastic compliance at final temperature,

$\underset{\sim}{M}^{es}$ = Elastic compliance at starting temperature,

$\underset{\sim}{\sigma}^{s}$ = Stresses at starting point,

$\underset{\sim}{\delta}^{fs}$ = Change in free thermal expansion from starting temperature to final temperature,

$\underset{\sim}{\dot{\epsilon}}^{P}$ = Total plastic strain increment,

$\underset{\sim}{M}^{P}$ = Plastic compliance,

$\underset{\sim}{\dot{\epsilon}}^{pT}$ = Plastic strain increment due to temperature change.

The explicit forms of $\underset{\sim}{M}^{P}$ and $\underset{\sim}{\dot{\epsilon}}^{pT}$ are derived in the Appendix.

Equation (5) can be recast into a more convenient form which is valid for both elastic and plastic loading cases.

$$\underset{\sim}{\dot{\epsilon}}_{(r)} = \underset{\sim}{M}_{(r)}\ \underset{\sim}{\dot{\sigma}}_{(r)} + \underset{\sim}{\dot{\epsilon}}^{T}_{(r)}. \tag{8}$$

(r = f for fibers and m for matrix)

where

$$\underset{\sim}{M}_{(r)} = \underset{\sim}{M}^{ef}_{(r)} + \underset{\sim}{M}^{p}_{(r)}, \tag{9}$$

and

$$\dot{\underset{\sim}{\epsilon}}^{T}_{(r)} = \dot{\underset{\sim}{\epsilon}}^{eT}_{(r)} + \dot{\underset{\sim}{\epsilon}}^{pT}_{(r)}. \tag{10}$$

Substituting the constitutive relation (8) into equation (4), and making use of equations (1) and (2) to eliminate $d\sigma_{ij}^{(f)}$ and $d\sigma_{ij}^{(m)}$ except for $d\sigma_{11}^{(m)}$. The resulting form is, after rearranging the terms,

$$d\sigma_1^{(m)} = (\sum_{j=1}^{6} B_{1j}^{(m)}\, d\sigma_j) + b_1^{(m)} \tag{11}$$

where

$$\begin{aligned} B_{11}^{(m)} &= M_{11}^{(f)} / (c_f h), \\ B_{1j}^{(m)} &= (M_{1j}^{(f)} - M_{1j}^{(m)}) / h; \text{ for } j = 2, 3, 4, 5, 6, \\ b_1^{(m)} &= (\dot{\epsilon}^{T}_{1(f)} - \dot{\epsilon}^{T}_{1(m)}) / h, \\ h &= (M_{11}^{(m)} + \frac{c_m}{c_f} M_{11}^{(f)}). \end{aligned} \tag{12}$$

Note that $M_{1i}^{(f \text{ or } m)}$, i = 1, 2, 3, 4, 5, 6, are the first row components of the matrix $\underset{\sim}{M}^{(f \text{ or } m)}$ defined by equation (9), and $\dot{\epsilon}^{T}_{1(f \text{ or } m)}$ is the first component of the vector $\dot{\underset{\sim}{\epsilon}}^{T}_{(f \text{ or } m)}$ defined by equation (10).

Now, equations (1) and (11) enable us to relate the matrix stress increment $\dot{\underset{\sim}{\sigma}}_{(m)}$ to the overall composite stress increment $\dot{\underset{\sim}{\sigma}}$ and the temperature change.

$$\dot{\underset{\sim}{\sigma}}_{(m)} = \underset{\sim}{B}_{(m)}\, \dot{\underset{\sim}{\sigma}} + \underset{\sim}{b}_{(m)}. \tag{13}$$

where $\underset{\sim}{B}_{(m)} = \begin{bmatrix} B_{11}^{(m)} & B_{12}^{(m)} & B_{13}^{(m)} & B_{14}^{(m)} & B_{15}^{(m)} & B_{16}^{(m)} \\ 0 & 1 & 0 & 0 & 0 & 0 \\ 0 & 0 & 1 & 0 & 0 & 0 \\ 0 & 0 & 0 & 1 & 0 & 0 \\ 0 & 0 & 0 & 0 & 1 & 0 \\ 0 & 0 & 0 & 0 & 0 & 1 \end{bmatrix}$

and $\underset{\sim}{b}_{(m)} = [\, b_1^{(m)} \quad 0 \quad 0 \quad 0 \quad 0 \quad 0 \,]$

Naturally, one can expect a similar relationship to exist for fibers, i.e.,

$$\dot{\underset{\sim}{\sigma}}_{(f)} = \underset{\sim}{B}_{(f)}\, \dot{\underset{\sim}{\sigma}} + \underset{\sim}{b}_{(f)}. \tag{14}$$

For a binary material system, the local averages and overall stress and strain increments are related by

$$\dot{\underset{\sim}{\sigma}} = c_m\, \dot{\underset{\sim}{\sigma}}_{(m)} + c_f\, \dot{\underset{\sim}{\sigma}}_{(f)}, \tag{15}$$

$$\dot{\underset{\sim}{\epsilon}} = c_m\, \dot{\underset{\sim}{\epsilon}}_{(m)} + c_f\, \dot{\underset{\sim}{\epsilon}}_{(f)}. \tag{16}$$

Substituting equations (13) and (14) into equation (15), one finds the following two relations,

$$c_m\, \underset{\sim}{B}_{(m)} + c_f \underset{\sim}{B}_{(f)} = \underset{\sim}{I}, \tag{17}$$

$$c_m\, \underset{\sim}{b}_{(m)} + c_f \underset{\sim}{b}_f = \underset{\sim}{0}. \tag{18}$$

where $\underset{\sim}{I}$ is a 6x6 identity matrix and $\underset{\sim}{0}$ is a 6x1 null vector. Thus, $\underset{\sim}{B}_{(f)}$ and $\underset{\sim}{b}_{(f)}$ can be found easily once $\underset{\sim}{B}_{(m)}$ and $\underset{\sim}{b}_{(m)}$ are known.

Finally, if one writes the macroscopic composite stress-strain relations in the usual manner

$$\underset{\sim}{\dot{\varepsilon}} = \underset{\sim}{M}\,\underset{\sim}{\dot{\sigma}} + \underset{\sim}{\dot{\varepsilon}}^{T}, \tag{19}$$

and note that with the help of equations (8), (13), and (14), equation (16) can be rewritten in a form comparable to equation (19). Hence, the composite compliances $\underset{\sim}{M}$ and $\underset{\sim}{\dot{\varepsilon}}^{T}$ can be identified as

$$\underset{\sim}{M} = c_m\,\underset{\sim}{M}_{(m)}\,\underset{\sim}{B}_{(m)} + c_f\,\underset{\sim}{M}_{(f)}\,\underset{\sim}{B}_{(f)} \tag{20}$$

$$\underset{\sim}{\dot{\varepsilon}}^{T} = c_m(\underset{\sim}{M}_{(m)}\,\underset{\sim}{b}_{(m)} + \underset{\sim}{\dot{\varepsilon}}^{T}_{(m)}) + c_f(\underset{\sim}{M}_{(F)}\,\underset{\sim}{b}_{(f)} + \underset{\sim}{\dot{\varepsilon}}^{T}_{(f)}) \tag{21}$$

In the case of pure elastic deformation of either phases, equations (20) and (21) are still applied providing that the compliances of the elastically deformed phase or phases be set to zero. This is equivalent to letting $H_{(r)} = \infty$ in equations (A-13) and (A-14) in the Appendix.

Equations 19 to 21 completely describe the instantaneous thermomechanical stress-strain relations of the MT composites. However, despite the simplicity of the mathematical expressions, the compliances $\underset{\sim}{M}$ and $\underset{\sim}{\dot{\varepsilon}}^{T}$ have to be evaluated numerically from equations (20) and (21). Because the plastic compliances of the phases, $\underset{\sim}{M}_{(f,m)}$, $\underset{\sim}{\dot{\varepsilon}}^{T}_{(f,m)}$, as well as the factors $\underset{\sim}{B}_{(f,m)}$ and $\underset{\sim}{b}_{(f,m)}$ are dependent upon the unknown stress averages of the phases at the final stress state.

ANALYSIS OF LAMINATED MT COMPOSITES

As noted previously, a computer code "EPLAM" was developed earlier by MSC staff to perform incremental elastoplastic stress analyses of laminated plates [ ]. To analyze laminated MT composites, the extended VFD model derived in the previous section was programmed into a subroutine that could provide the main program "EPLAM" with the instantaneous stress-strain relation of each microstructurally toughened lamina. EPLAM was then able to perform a nonlinear laminate analysis to determine the overall behavior of a laminated MT composite plate.

The significance of this analysis is that it not only gives us the ability to deal with laminated MT composites which is expected in the future plan of material development, but also provides us with a convenient tool to analyze a MT composite with sparsely populated toughening tubes. In this case, the MT composite can be idealized as a system of alternating layers of toughening tubes and particulate reinforced region (fig. 2b).

MODELING OF IMPACT DAMAGE AND WORK OF FRACTURE

The high fracture toughness is the most important advantage that the MT composites have over the conventional particulate reinforced metal matrix composites. The impact energy absorption data of the MT composites were obtained in [5] by conducting a series of instrumented Charpy impact tests. The shape and dimensions of the MT composite specimens used in the test are shown in Figure 3. A detailed description of the testing procedure can be found in [5].

The impact energy absorption data of SiCp/6061 Al based MT composites are tabulated in Table 2 which includes three different toughening approaches, namely, (1) SiCp/6061 Al rods toughened by continuous 6061 Al region (fig. 4a), (2) SiCp/6061 Al continuous region toughened by 6061 Al tubings (fig. 4b), (3) SiCp/6061 Al continuous region toughened by CP titanium tubings (fig. 4c).

Table 2 clearly indicates that changing the material composition as well as varying the geometric shapes and dimensions of the toughening region can have profound effects on the impact damage absorption capabilities of the MT composites. Therefore, modeling effort should account for both the material properties and the geometric details. This is in contrast to the usual practice of modeling fibrous composites in which the geometric details other than the volume fractions of the phases are ignored. To make the matter even more complicated, the impact damage is dynamic in nature and there is no doubt that the modeling of dynamic effects on elastoplastic heterogeneous materials will entail tremendous difficulties.

In this study, we have chosen a different approach. We have made an attempt to find a quantitative criterion for whether or not the toughening mechanism could become operative during impact damage process. We believe that this criterion will be essential in achieving a successful MT composite design

such that the toughening effects provided by the toughening region materials can be fully utilized. The treatment is by no means rigorous but it has the advantage of producing a quantitative criterion in terms of the material and geometric variables of the MT composites. This modeling attempt will be described next.

An extremely simple case of a simply supported composite beam under plastic collapse load is considered in Figure 5a. Recall that both phases of the MT composite are ductile materials, therefore, the collapse load as calculated by plastic limit analysis of beams can be written as [11]:

$$F_{clp} = 2M_y / \ell. \tag{22}$$

ℓ is one-half of the beam span, and M_y is the yield moment which, if both the reinforced and toughening regions are uniformly distributed over the cross-sectional area, can be calculated as:

$$M_y = \frac{ab^2}{4} [V_{(r)} \sigma_{ult}^{(r)} + V_{(t)} \sigma_{ult}^{(t)}], \tag{23}$$

where a,b = dimensions of the cross-sectional area as shown in Figure 5b,

$V_{(r)}$, $V_{(t)}$ = volume fractions of the reinforced and toughening regions, respectively,

$\sigma_{ult}^{(r)}$, $\sigma_{ult}^{(t)}$ = the material ultimate strengths of the reinforced and toughening regions, respectively.

It should be noted that in this section the indices (r) and (t) are used to denote the reinforced region and the toughening region, respectively.

Assuming the final failure occurs when the mid-span deflection of the beam reaches a maximum value Δ, then, the energy absorbed by the beam up to the time of failure is equal to the external work done by the collapse load, i.e.,

$$\bar{W} = F_{clp} \cdot \Delta \tag{24}$$

The principle assumption in this treatment is that we assume the same beam will have absorbed the same amount of energy at failure should it be subject to impact loads. At present, there is no experimental evidence available to support or dispute this assumption. However, by judging from the fact that the strength of most structural materials increases at high strain rates, the MT composites possibly can absorb more energy in impact than in static loads.

As a first order estimate of the maximum beam deflection Δ at mid-span, we adopt the strain-deflection relation that can be derived from an elastic deflection curve, i.e.,

$$\epsilon_{max} = \frac{3b}{2\ell^2} \Delta \text{ , at center } (z=0). \tag{25}$$

Making use of equation (25), one can define two limiting mid-span deflections,

$$\Delta_1 = \epsilon_{max}^{(r)} / (\frac{3b}{2\ell^2}) \tag{26}$$

$$\Delta_2 = \epsilon_{max}^{(t)} / (\frac{3b}{2\ell^2}) \tag{27}$$

where $\epsilon_{max}^{(r)}$ and $\epsilon_{max}^{(t)}$ are the tensile failure strains of the reinforced and toughening region materials, respectively.

It can be understood that Δ_1 is the mid-span deflection at which the outermost reinforced region material begins to fail, and Δ_2 is the mid-span deflection at which the outermost toughening region material begins to fail. Since $\epsilon_{max}^{(t)} > \epsilon_{max}^{(r)}$ is always true for MT composites, the outermost reinforced region material will fail first. At this initial stage of failure, the energy absorbed by the beam is

$$\bar{W}_1 = F_{clp} \cdot \Delta_1 \tag{28}$$

Next, we should investigate how the initial failure of the reinforced region could affect the integrity of the outermost toughening region material. A schematic representation of this interaction between these two regions is shown in Figure 6. If two regions are totally disbonded as shown in Figure 6a, the failing of reinforced material can result in a elastic unloading and the reinforced region will shrink by an amount equal to $\sigma_{ult}^{(r)} \ell / E_{(r)}$. This motion of shrinkage is toward the end-support of the beam and it does not drag the toughening region to go along because the two regions are totally disbonded.

However, if the two regions are bonded, an interfacial shear zone will develop over a distance ℓo along the interface (fig. 6b). The length of the shear zone can be determined by a simple shear lag model and by assuming the shear stress in the shear zone is uniform and is equal to τ_s. If one chooses to match the axial displacements $U_{(r)}$ and $U_{(t)}$ at $z=\ell o$, one has

$$U_{(r)} = [\sigma_{ult}^{(r)} - \frac{\tau_s S \ell o}{A_{(r)}}] \frac{(\ell - \ell o)}{E_{(r)}},$$

$$U_{(t)} = \frac{\tau_s S \ell o}{A_{(t)} E_{(r)}} (\ell - \ell o), \tag{29}$$

where

S : perimeter of the interface boundary

$A_{(r)}$, $A_{(t)}$: cross-sectional areas of the reinforced and toughening regions, respectively

Equating $U_{(r)}$ with $U_{(t)}$ gives

$$\ell o = \frac{\sigma_{ult}^{(r)}}{C \tau_s} \left(\frac{E_{(r)}}{E_{(t)}} + \frac{V_{(t)}}{V_{(r)}}\right)^{-1} \tag{30}$$

where

$$C = S / A_{(t)}. \tag{31}$$

Simplified expressions of C for three simple cases can be found in Figure 7. Since ℓo can not be exceeding ℓ, therefore, ℓo is the minimum value of the two, i.e.,

$$\ell o = \text{Min.}\ [\frac{\sigma_{ult}^{(r)}}{C\tau_s}(\frac{E_{(r)}}{E_{(t)}} + \frac{V_{(t)}}{V_{(r)}})^{-1},\ \ell] \tag{32}$$

Consequently, the interfacial shear stress causes the toughening region to shorten by an amount equal to

$$\Delta\ell = \frac{C\tau_s}{E_{(t)}}\ [\ell o(\ell - \frac{\ell o}{2})]. \tag{33}$$

To maintain the integrity of the toughening region, an additional plastic flow must be generated in the toughening region material in order to compensate for this shortening. Since for $z>\ell o$, the toughening region will be unloaded back to elastic state by the interfacial shear stress, the plastic flow can occur only within the $0<z<\ell o$ segment. The average plastic strain increment within this segment is thus

$$\Delta\epsilon_p^{(t)} = \Delta\ell/\ell o = \begin{cases} \dfrac{C\tau_s \ell}{E_{(t)}} - \dfrac{V_{(r)}\sigma_{ult}^{(r)}}{2(V_{(r)}E_{(r)} + V_{(t)}E_{(t)})} & \text{if } \ell o < \ell \\ \dfrac{C\tau_s \ell}{2E_{(t)}} & \text{if } \ell o = \ell \end{cases} \tag{34}$$

It is now clear that the initial failure of the outermost reinforced region material would result in an additional plastic strain increment, i.e., $\Delta\epsilon_p^{(t)}$ in equation (34), in the outermost toughening region material. Consequently, the toughening region material could fail at once if

$$\epsilon_{max}^{(r)} + \Delta\epsilon_p^{(t)} \geq \epsilon_{max}^{(t)}. \tag{35}$$

If this is the case, the beam will fail when the outermost reinforced region material starts to fail and, therefore, no toughening effects can be realized. The fracture energy of the beam in this case is equal to $\bar{\Gamma}_i$ (equation 28).

On the other hand, the beam will continue to deform if the toughening region is able to withstand this additional straining, i.e.,

$$\epsilon_{max}^{(r)} + \Delta\epsilon_p^{(t)} < \epsilon_{max}^{(t)}. \tag{36}$$

But, instead of reaching a mid-span deflection Δ_2 as calculated by equation (27), the outermost toughening region material will fail when the mid-span deflection of the beam reaches

$$\Delta = (\epsilon_{max}^{(t)} - \Delta\epsilon_{p}^{(t)}) \; / \; [\frac{3b}{2\ell^2}]. \tag{37}$$

The fracture energy of the beam in this case is then

$$\bar{W} = F_{clp} \cdot \Delta, \tag{38}$$

where Δ is given by equation (37).

Equation (36) is the criterion for toughening mechanism to become active during impact damage process. If it does become active, the fracture toughness of the MT composite will increase from $\bar{W}_1$ (equation 28) to $\bar{W}$ (equation 38).

STRUCTURAL COMPONENT SELECTION

Two structural components were identified as possible designs that can be improved through the use of MT composites. The selection was based upon a survey of structural components that are of interest to SDI, and also upon interviews with SDI, ONR and UTRC personnel. These selected structural components are a submarine hull and the lower longeron for the Supportable Hybrid Fighter Structure (SHFS).

Aircraft Longeron

The lower longeron, shown in Figures 8 and 9, is part of a fighter aircraft fuselage which is located immediately forward of the wing carry-through structure. It is loaded primarily by fuselage bending and is designed to meet limit load requirements, ultimate load requirements, and a specified fatigue lifetime. The component geometry and loading conditions were provided by General Dynamics, Fort Worth Division.

The present design calls for the structure to be made from homogeneous SiC Al material. This may prove to be an attractive applicant for MT composites because of the life time requirements and the fact that it is a relatively large component. The preliminary design of this component will be discussed later.

Submarine Hull

Another area of current Navy research has focused on the application of composite materials to submersible structures. These structures can be classified, by loading environment, as pressure hull and non-pressure hull structures. Both classes of structure are subjected to a seawater environment, however the pressure hull structure defines the water tight envelope and must support the external pressure induced by submergence. Candidate pressure hull materials must have a very high modulus to preclude elastic stability failures. Graphite epoxy materials are emerging as the leading candidate for composite submersible pressure hull applications.

Non-pressure hull structures are free-flooding or water backed structures subjected to working loads other than submergence pressure. These structures provide support for external propulsion and sonar systems, and serve as ballast tank (bow and stern) structures. This class of structure also includes the hydrodynamic appendages, or bow and stern steering and diving planes. Microstructurally toughened SiC/Al composite materials may be a high pay-off candidate for non-pressure hull structure applications.

Non-pressure hull structures have traditionally been designed to include the effects of post-yield strength of the material. The high yield strength and excellent ductility of the microstructurally toughened SiC/Al composites make these materials very attractive for non-pressure hull applications. Weight is a major design constraint because of the location (at the extreme for and aft ends of the submersible) of non-pressure hull structures. The low density of the SiC/Al composite (less than half of that of steel) would result in a structural weight reduction which could translate to increased equipment payload, speed or diving depth. Maintainability is a paramount concern in the ballast tank area, therefore the non-corrosive nature of Sic is a distinct advantage over steel. The non-magnetic signature of SiC would also be a

benefit if acoustic detectability or stealth were a consideration (i.e. combatant submarines).

RESULTS

The results presented here include discussions of the material properties; the predictions of stress-strain constitutive relations; the analyses of laminated MT composites; the estimations of impact damage and work of fracture; the optimization of impact damage resistance; and the initial results of the preliminary design for the SHFS lower longeron.

MATERIAL PROPERTIES

The base material for the MT composites studied in this report is the SiC particulate reinforced Al 6061 material. Three toughening approaches were investigated in this report (see Figure 4). They are: (1) a continuous aluminum 6061 toughening region, (2) aluminum 6061 toughening tubes, and, (3) CP titanium toughening tubes. The properties of each individual material were obtained in [5] by tensile testing. It should be noted that prior to tensile testing heat treatment and consolidation were applied to the precursor materials in the identical manner as in the extrusion process of the MT composites.

A summary of the material property data was provided in [5] and has been reproduced here in Table 1. Note that there are three SiCp/Al 6061 materials in Table 1. They differ in the volume fractions of SiC particles and also differ in the way that they were fabricated. The specific compositions and geometries of the MT composites studied in this report are tabulated in Table 2. The Table shows a total of 8 MT composites, and each material has been designated a material number. For simplicity, the individual MT composite will be referenced by its designated number.

STRESS-STRAIN CONSTITUTIVE RELATIONS

The extended VFD model was used to calculate the axial stress-strain relations of the MT composites. For simplicity, the nonlinear stress-strain behaviors of the constituents were idealized by using an elastic-linear strain hardening law which could be represented by a bilinear curve as the one that is shown in Figure 10.

Figures 11 and 12 are the predicted axial stress-strain curves of the No. 2 and No. 4 MT composites. Both materials apparently failed when the reinforced region materials reached their respective maximum strains. Therefore, the tensile strengths of both MT composites did not benefit from the presence of toughening region material which was Al 6061 in both cases. This is probably due to the fact that Al 6061 has lower tensile strength than the SiCp/Al 6061 material. Hence, when the relatively brittle SiCp/Al 6061 started to fail, the load transferring process simply overstressed the remaining Al 6061 material.

It is reasonable to assume that in order to improve the ductility and static tensile strength of MT composites one has to select a toughening region material which has higher tensile strength than the reinforced region material. A good example is the CP titanium toughening tubes that were used in the Nos. 6, 7 and 8 MT composites. It can be seen from Table 2 that the failure strengths and strains of these three MT composites all showed improvement over the corresponding values of the reinforced region material which was the UTRC fabricated SiCp/Al 6061 material. In fact, the impact damage absorption capabilities of MT composites will also be enhanced by using toughening materials which have higher tensile strengths. This will be discussed in more detail later.

The influence of interfacial bonding strength on the tensile strength of the MT composites can be observed from Table 2 as well. Both No. 2 and No. 3 MT composites had samples prepared by different surface treating methods. The acid cleaning method was used to promote strong interfacial bonding while the acid cleaning plus debonding agent was used to promote weak interfacial bonds. The samples with strong interfacial bonds were shown to have slightly higher tensile strengths and tensile failure strains.

The indication is that strong bonding allows for stress transferring process to be carried out more efficiently in a cracked MT composite system. The bridging effect works in the same manner as in the case of fiber reinforced composites containing matrix cracks. However, the effect is quite small in the case of MT composites where the ultimate strengths of the constituents are not that much different. Consequently, a detailed study of this effect was excluded from the limited Phase I work plan.

Figure 13 is the predicted axial shear stress-strain behavior of the No. 2 MT composite. No experimental data point was plotted with this curve because there is no data currently available. This illustrated the usefulness of material modeling because unavailable material properties can always be estimated. In addition, the effects of alternate materials and volume fractions can also be evaluated with ease by material modeling.

For MT composites with low concentration of toughening tubes, there might be a considerable amount of reinforced region material gathering in between adjacent tubes. An incremental laminate analysis was made available to cope with this situation (see Figure 2b). On the other hand, this material could also be approximated by a single cylindrical assemblage but with a larger O.D. such that all the reinforced region material can be accommodated within this enlarged tube.

These two different approaches were used to analyze the axial stress-strain behavior of the No. 6 MT composite. But, instead of using 0.51 for the volume fraction of the toughening tubes, a lower volume fraction of 30% was selected to better represent the case of low volume concentration of toughening tubes. Figure 14 shows that axial stress-strain curves predicted by both approaches do not have significant differences. This implies that the laminate analysis is not needed if the No. 6 MT composite has more than 30% volume fraction of toughening tubes. However, this conclusion might not be valid for MT composites with different material compositions.

LAMINATED MT COMPOSITES

As shown previously, the laminate analysis has given us a tool to deal with MT composites which might have low volume concentration of toughening tubes. In addition, this analysis also gives us the ability to analyze laminated MT composites. Figure 15 shows the comparison between three different laminations of the No. 2 MT composite. The very much isotropic nature of the No. 2 material renders the similarity of all three axial stress-strain curves.

It appears that there is very little to gain by laminating the MT composites. However, as will be discussed in the following section, the impact damage resistance of MT composites can be improved by having a weaker bonding

between the reinforced and toughening region materials. It is expected that a weaker interfacial bonding can severely degrade the transverse properties of the MT composites. Therefore, lamination could well be a viable method for compensating this degradation and, thus, allowing for the construction of a high impact energy absorbing MT composite without sacrificing the integrity of its transverse properties.

ANALYSES OF IMPACT DAMAGE AND WORK OF FRACTURE

A crude model for estimating the impact damage absorbing capability of MT composites was developed in the Approach section. The initial goal was to identify a quantitative criterion for whether or not the toughening mechanism could become operative during impact damage process. Equation (36) was found to be such a criterion. If the criterion is satisfied, the MT composite will attain a fracture toughness which can be calculated from equation (38), otherwise the fracture toughness will be given by equation (28).

However, the application of equation (38) requires a knowledge of the interfacial shear strength τ_s. Since τ_s is unknown at present time, it can only be estimated by a data correlation procedure.

The procedure is straightforward. By assuming τ_s varies from 0 to 30 ksi, the corresponding fracture toughness can be computed either from equation (38) or from equation (28). A representative τ_s can then be estimated by correlating the experimentally measured toughness data with the calculated toughness-Interfacial shear strength curve.

Figure 16 shows a typical toughness-interfacial shear strength curve. The material involved is the No. 1 MT composite. This curve indicates that for an interfacial shear strength greater than 5 ksi, initial failure of the reinforced region material in this MT composite will always overstrain the toughening region material to failure at the same time. In this case, the toughening region material will be unable to increase the toughness of the MT material. On the other hand, if the interfacial shear strength can be brought down to below 5 ksi, then, the toughening region will start to make its presence shown by increasing the toughness up to a maximum value of 7 ft-lbs.

A toughness of 3.9 ft-lbs was measured for this material. This value is even lower than the lowest prediction in Figure 16 which is slightly higher

than 10 ksi. This low toughness was probably due to the notch effect that came as a direct consequence of the prenotched specimen. Since the impact damage model does not account for notch effects, the only meaningful conclusion that we can draw from this data correlation is that the actual interfacial shear strength was greater than 5 ksi. Thus, when the reinforced region material failed prematurely due to notch effect, the overstraining brought the toughening tubes to fail simultaneously.

Figures 17 and 18 show the data correlation results for the No. 2 and No. 3 MT composites. Note that there were two toughness data points measured for each of these two MT composites. The pair of higher toughness values were the result of a weaker interfacial bonding for which a debonding agent was applied over the SiCp/6061 Al rod surfaces before the MT composites were fabricated. In relation to the higher toughness values, an interfacial shear strength of 2.5 ksi can be identified from both figures. However, the pair of measured low toughness data are again lower than the lowest predictions on both figures.

The two conclusions which can be drawn from Figures 17 and 18 are:

(1) Without debonding agent, the interfacial shear strengths were higher than 5 ksi in both cases. Therefore, when the reinforced region failed prematurely due to the notch effect, they brought the toughening regions and the MT composites to fail at the same time.

(2) By applying the debonding agent, the interfacial shear strength was brought down to 2.5 ksi. Due to this weaker bonding, the toughening mechanism was allowed to be operative after the initial failure of the reinforced region material had occurred. The result was a much improved fracture toughness for each material.

When applying the same data correlation scheme to other MT composites, the additional remarks can be made:

(3) No. 4 and No. 5 MT composites for which the Al 6061 tubings were the toughening region material, the interfacial shear strength was higher than 5 ksi. Hence, the toughening mechanism was unable to become operative and the material as a whole failed when the reinforced

region material failed due to the notch effect (see Figures 19 and 20).

(4) No. 6 and No. 7 MT composites for which the CP titanium tubings were the toughening region material, the interfacial shear strength can be found to be 7 ksi in relation to the measured toughness values (see Figures 21 and 22).

Note that for the MT composites mentioned in the last two remarks, no debonding agent was applied to the tubing surfaces to promote weak interfacial bonding. Nevertheless, the CP titanium tubes were still able to raise the material toughness to a higher level while the Al 6061 tubes failed to lend any toughening effects to the reinforced region material. Recall CP titanium tubes also improved the static tensile strength of MT composites while Al 6061 tubes again failed to do the same. It appears now that titanium is a better choice for the toughening region material.

OPTIMIZATION OF IMPACT DAMAGE RESISTANCE

What we have learned from the previous data correlation study is that our crude model seemed to be able to furnish reasonable agreement with the test data providing that the interfacial shear strengths that were estimated by the model can be validated. In addition, we also learned that CP titanium is a better choice for toughening region material than Al 6061. However, even with CP titanium as the toughening region material, further improvement of fracture toughness is still possible. In the following we will use the No. 6 MT composite as an example to demonstrate various ways of improving its fracture toughness.

After a careful examination of equations (32) to (38) and a parametric study of this damage model, four possible ways of improving the material toughness were identified. Figure 23 shows an improved fracture toughness if one can increase the Young's modulus of titanium from 15.5 Msi to 28 Msi. The reason for this improvement is that a stiffer toughening region material can reduce the additional plastic straining that is brought upon it by the interfacial shear stress (see equation 34).

Figure 24 shows similar improvement of fracture toughness if one can increase the ultimate tensile strain of the titanium from 19% to 25%. The reason for this improvement is that the material can now experience larger deflection before the final failure occurs (see equation 37). It is worthwhile to point out that the titanium alloys can be tailored to achieve higher Young's modulus on the expense of a reduced ultimate tensile strain. Therefore, it is possible to use our model to find the best combination for these two variables such that the fracture toughness of the material can be optimized.

Aside from varying material properties, it is also possible to achieve higher fracture toughness by varying the geometries. Figure 25 shows the improved fracture toughness if one uses smaller but thicker titanium tubes such that the tube volume fraction remains unchanged. The use of thicker tubes implies a smaller value for the parameter C (see Figure 7a). A smaller C can reduce the additional plastic straining which would be brought upon the toughening region material by the interfacial shear stress (see equation 34). Therefore, a smaller parameter C promotes higher fracture toughness.

At the limit of a smaller but thickened tube, the tube becomes a solid rod. Figure 26 shows great improvement by using solid CP titanium rods instead of tubes. The improvement can be realized even when the interfacial shear strength is higher than 30 ksi. It is interesting to point out that recent UTRC experiments have confirmed this prediction. In their result (as shown in Table 3), 1/8 in. CP Ti rods were shown to have given the MT composite higher toughness than the 1/4 in. CP Ti tubes could. This result was achieved despite the fact that the volume fraction of the toughening region was only 25% for the solid rods and 30% for the tubes.

PRELIMINARY COMPONENT DESIGN

Recall that the lower longeron for the Supportable Hybrid Fighter Structure (SHFS), as shown in Figures 8 and 9, was selected as a potential structural component that can be improved through the use of MT composites. A preliminary design of this component will be described next. The component geometry and loading conditions were provided by General Dynamics, Fort Worth Division.

The 19 design loading cases, shown in Table 4, were used to compute the ultimate stresses shown in Table 5. The maximum and minimum normal stresses for each loading case were determined by

$$\sigma_{(\max,\ \min)} = \sigma^{\text{axial load}}_{(\max,\ \min)} + \sigma^{\text{bending load}}_{(\max,\ \min)} \tag{39}$$

where

$$\sigma^{\text{axial load}}_{(\max,\ \min)} = \text{axial load (max, min) / cross-sectional area,} \tag{40}$$

$$\sigma^{\text{bending load}} = \frac{M_1 x_p}{I_{yp}} + \frac{M_2 y_p}{I_{xp}}, \tag{41}$$

M_1, M_2 = the bending moments about the principal axes y_p and x_p, respectively;

I_{xp}, I_{yp} = the moment of inertias with respect to the principal axes x_p and y_p, respectively.

Equation (41) was used to compute the ultimate bending stresses at the four corner points, A, B, C, and D of the component cross-sectional area where the maximum and minimum bending stresses of the beam were most likely to occur (see Figure 9). The maximum and minimum values among the ultimate stresses at the four corner points were then selected as the maximum and minimum bending stresses of the beam.

The shearing stresses are of secondary concern. With a simple assumption that all of shear-1 was resisted by the area of the bottom flange and all of the shear-2 was resisted by the area of the right hand flange, the maximum shearing stress of the section was evaluated for each loading case. The results in Table 5 indicate that the shearing stresses are generally one order of magnitude smaller than the normal stresses.

From Table 5, the maximum tensile stress in the longeron is about 83 ksi and the maximum compressive stress is about 101 ksi. These strengths are attainable with a 35 volume percent SiCp/2124 SiCd/Al composites, reference 12. Therefore, a discontinuously reinforced metal matrix composite can be used to

construct a longeron which will meet the requirement of ultimate static strengths.

As for the fracture toughness consideration, a toughening mechanism composed of CP Ti solid rods was shown previously to have greatly enhanced the fracture toughness of the discontinuously reinforced SiCp Al 6061 materials. In addition, the relatively large size of the longeron beam will permit the use of larger CP Ti rods. As can be seen from Figure 7b, the geometric parameter C for toughening rods is inversely proportional to the rod diameter. Therefore, increasing the size of the rod will reduce the parameter C and further increase the fracture toughness of the material.

However, as far as static strength is concerned, the ultimate strength of CP titanium is 70 ksi which is lower than the required strength of the longeron. Therefore, even though high strength SiCp/Al 6061 material can be obtained by increasing the volume fraction of the particulate reinforcement, the addition of CP Ti rods will decrease the material static strength and might even make the material less ductile as explained in the section of stress-strain predictions. It appears now the longeron construction will require a new toughening region material which should have a strength of at least 100 ksi.

This example demonstrated the need for further MT material development. More suitable toughening region materials have to be identified and tested. One possible candidate is the titanium alloy Ti-6Al-4V which has an ultimate strength of 163 ksi at room temperature.

CONCLUSIONS AND RECOMMENDATIONS

The results of this Phase I study have led to several important conclusions regarding the material design of MT composites. This program resulted in the creation of an extended VFD material model that was capable of approximating the axial stress-strain response reasonably well. The model is also capable of handling material nonlinear strain hardening, temperature dependent material properties, and very general loading path which might include thermal loads. The extended VFD model was further incorporated into an existing MSC computer code which was originally developed for elastoplastic laminate analysis. This new software has given us the ability to analyze laminated MT composites. The program also resulted in the development of a crude impact damage model which was proven to be useful in the understanding of the effects of toughening mechanisms at micromechanics level. A preliminary design example was performed for an aircraft longeron beam, and the result brought up the need for identifying more high strength toughening region materials.

The stress-strain data correlation has suggested the following general guideline for MT composite strength design. For higher ultimate strength and more material ductility, the toughening region material should have higher ultimate strength as well as higher failure strain relative to the reinforced region material. Strong interfacial bond also helps to raise the ultimate strength and ductility of the MT composites. But the improvement is not significant.

For achieving higher impact damage resistance, the impact damage data correlation has suggested the following guidelines for MT composite toughness design.

(1) From the material property aspect, the toughening region material should have higher ultimate strength, higher failure strain, and higher stiffness as compared to the reinforced region material.

(2) From the geometry aspect, the form of toughening region must ensure a small geometric parameter C (see Equation 31). This implies that thicker tubes are

better than thinner ones; solid rods are better than tubes; and larger rods are better than smaller rods.

(3) From the interfacial bonding aspect, weaker bonding promotes much higher fracture toughness. The improvement is so great that the slightly decreased static strength and ductility of the MT composites as the results of a weak interfacial bonding can be considered justifiable.

The preliminary design of the lower longeron structural component showed that a discontinuously reinforced SiC/Al 6061 material can be found to meet the static strength requirements. However, an appropriate toughening region material for the longeron structure was found to require higher ultimate strength than both aluminum 6061 and CP titanium can offer. Therefore, there is a demand for identifying additional toughening region materials with ultimate strengths no less than 100 ksi.

The MT composites have many fascinating properties and a very promising future. The Phase I study assessed the merits of the MT composites on a micromechanics level. Several recommendations can be made which should be considered for the Phase II program. Future efforts should focus on characterizing the behavior of MT composites on a structural level. This will include, as a minimum, studies of the effects of holes and other discontinuities, and the effects of general loading conditions including cyclic loads. A structural component will be selected. This component might be the longeron beam which was selected in Phase I study, or other more appropriate components. Detailed designs will be performed to specify the structure configuration, material composition, the joining method which will be used to attach the component to the main structure and finally, the fabrication and testing of a subscale component to assess the design methodology.

REFERENCES

1. McDaniels, D. L., "Analysis of Stress-strain, Fracture and Ductility Behavior of Aluminium Matrix Composites Containing Discontinuous Silicon Carbide Reinforcement", Metall. Trans., 16A, 1985, P.1105.

2. Schuster, D. M., and Skibo, M. D., "Low-Cost Discontinuously Reinforced SiC-Al Fabricated by Casting", Proceedings of Sixth Metal Matrix Composites Technology Conference, Naval Postgraduate School, Monterey, CA, May 1985, p.27-1.

3. Heimann, T. H., Gubbay, J. D., and Hall, E. J., "Discontinuously Reinforced MMC for Missile Guidance Hardware", Proceedings of Seventh Metal Matrix Composites Technology Conference, NSWC, Silver Spring, Maryland, May 1987, p.15-1.

4. DiGiovanni, P. R., Franceschi, L. and Rosenberg, E. M., "Development of a Discontinuously Reinforced SiC/Al Tactical Missile Wing", Proceedings of Seventh Metal Matrix Composites Technology Conference, NSWC, Silver Spring, Maryland, May 1987, p.17-1.

5. Nardone, V. C. and Strife, J. R., "Development of Microstructurally Toughened Composites", UTRC Annual Report For ONR Contract N00014-87-C-0406, August, 1989.

6. Chatterjee, S. N., and Wung, E. C. J., "Software Development for Matrix Composite Material Evaluation", Technical Final Report. MSC TFR 1816/8304, Contract No. N00164-87-C-0233, NWSC, Crane, Indiana, January 1988.

7. Barrett, D. J., and Buesking, K. W., "Temperature Dependent Nonlinear Metal Matrix Laminate Behavior", NASA Contract Report 4016 on NASA Contract NAS1-17822, September, 1986.

8. Dvorak, G. J., and Bahei-El-Din, Y. A., "Plasticity Analysis of Fibrous Composites", Journal of Applied Mechanics, Vol. 49, pp. 327-335, June, 1982.

9. Hashin, Z., "Thermoelastic Properties of Fiber Composites with Imperfect Interface", Mechanics of Materials, 8, pp. 333-348, 1990.

10. Ziegler, H., "A Modification of Prager's Hardening Rule", Quarterly of Applied Mathematics, Vol. 17, pp. 55-65, 1959.

11. Hodge, P.G., Jr., "Plastic Analysis of Structures", McGraw-Hill Book Company, Inc., New York, 1959.

12. Misra, M. S. and Rawal, S. P. "Composite Materials for Space Applications", NAS1-18230, Martin Marietta report MCR-87-636, July 1988.

Table 1. Tensile Properties Of MT Composite Precursor Materials

Material	Elastic Modulus (Msi)	Yield Strength (ksi)	Ultimate Tensile Strength (ksi)	Failure Strain (%)	Area Under Stress–Strain Curve (ksi)
25% SiCp/6061Al (DWA Fabricated)	16.4	57.8	67.2	5.8	3.6
30% SiCp/6061Al (DWA Fabricated)	17.4	53.4	63.0	4.8	3.2
30% SiCp/6061Al (UTRC Fabricated)	16.4	47.1	52.3	3.0	1.5
6061AL (Powder Metallurgy)	10.0	46.8	50.7	12.9	6.7
CP Titanium	15.5	53.3	70.0	19.0	16.1

Table 2. Test Data For Various MT Composites

MT Composite Designated Number	Reinforced Region Precursor		Toughening Region Precursor		Surface Treatment	Average Impact Energy (ft.lbs)	Average Tensile Strength (ksi)	Average Tensile Failure Strain (%)
	Material	V_r	Material	V_t				
1	3/8 in. OD Rods 25% SiCp/6061Al (DWA Fabricated)	0.83	6061Al Powder	0.17	Acid * Cleaned	3.9	56.2	6.0
2	1/4 in. OD Rods 30% SiCp/6061Al (DWA Fabricated)	0.75	6061Al Powder	0.25	Acid Cleaned	2.5	59.8	4.3
					Acid ** Cleaned & Debonding Agent	16.3	57.0	3.9
3	3/16 in. OD Rods 30% SiCp/6061Al (DWA Fabricated)	0.76	6061Al Powder	0.24	Acid Cleaned	1.5	55.5	6.0
					Acid Cleaned & Debonding Agent	12.9	52.3	4.0
4	30% SiCp/6061Al (UTRC Fabricated)	0.58	1/4" ODx0.028" Wall 6061Al Tubes	0.42	Acid Cleaned	2.5	47.5	2.4
5	30% SiCp/6061Al (UTRC Fabricated)	0.47	3/16" ODx0.030" Wall 6061Al Tubes	0.53	Acid Cleaned	2.9	44.7	2.2
6	30% SiCp/6061Al (UTRC Fabricated)	0.49	1/4" ODx0.035" Wall CP Ti Tubes	0.51	Solvent # Cleaned	21.5	61.5	8.6
7	30% SiCp/6061Al (UTRC Fabricated)	0.59	0.186" ODx0.019" Wall CP Ti Tubes	0.41	Solvent Cleaned	5.9	63.8	5.3
8	30% SiCp/6061Al (UTRC Fabricated)	0.70	0.23" ODx0.019" Wall CP Ti Tubes	0.30	Solvent Cleaned	4.4	63.2	4.1

* Acid cleaning to promote strong interfacial bond

** Acid cleaning and debonding agent to promote weak interfacial bond

Solvent cleaning also promotes strong interfacial bond

Table 3. Comparison of Toughening Effects Between CP Ti Rods And Tubes

Toughening* Region Form	Toughening Region Diameter (in)	Toughening Region Volume Fraction	Notched Impact Energy (ft.lbs)
Tube	1/4	0.30	4.4
Rod	1/8	0.25	7.6

* The reinforced region material is the UTRC fabricated SiCp/6061 Al

Table 4. SHFS Longeron Design Loads

ELEMENT SET 1 (CONTINUED)
SHFS COMPONENET LOWER LONGERON AL SOMANATH, GENERAL DYNAMICS

ELEMENT TYPE ELEMENT ID NODE ID DATA TYPE DATA LOCATION LOAD CASE IDENTIFICATION	MINIMUM MOM-1	MAXIMUM MOM-1	MINIMUM MOM-2	MAXIMUM MOM-2	MINIMUM SHEAR-1	MAXIMUM SHEAR-1	MINIMUM SHEAR-2	MAXIMUM SHEAR-2	MINIMUM AXIAL	MAXIMUM AXIAL
LOADING CASE 1	14193	39930	-8511	10011	-891	469	-1160	1124	-123332	112007
LOADING CASE 2	-31944	-11355	-8009	6809	-375	713	-899	928	89606	98666
LOADING CASE 3	-4283	8607	-130	993	-435	417	-152	152	-1643	-1105
LOADING CASE 4	-392	189	-128	-9	-19	20	-13	13	-565	-532
LOADING CASE 5	-1088	1248	-427	859	-28	82	-110	42	-3043	-1602
LOADING CASE 6	-834	1158	-1280	703	-40	70	-164	63	2062	3079
LOADING CASE 7	-325	5124	-4665	1202	-233	246	-747	747	-4207	-2893
LOADING CASE 8	14095	39971	-8543	10009	-896	473	-1163	1127	-123473	112140
LOADING CASE 9	-31902	-11453	-8011	6777	-370	708	-896	925	89473	98524
LOADING CASE 10	22380	36275	-7550	10192	-485	42	-1011	1089	-125053	113614
LOADING CASE 11	13802	40097	-9638	10002	-910	488	-1173	1137	-124897	112549
LOADING CASE 12	-35598	-2846	-7828	7769	-802	1120	-1048	1077	88000	96951
LOADING CASE 13	-31777	-11746	-8018	6681	-355	694	-886	915	89074	98100
LOADING CASE 14	13111	39582	-8871	9676	-920	546	-1203	1166	-125036	115050
LOADING CASE 15	15352	39096	-7807	8731	-825	429	-1096	1059	-119732	109945
LOADING CASE 16	19316	39605	-13176	9473	-732	308	-1906	1871	-127539	111900
LOADING CASE 17	-32291	-12437	-8344	6140	-297	685	-890	885	86563	96296
LOADING CASE 18	-32778	-10196	-9289	7512	-414	700	-1015	991	91668	102335
LOADING CASE 19	-32269	-6232	-8547	2113	-547	896	-1036	448	96712	95090

Table 5. Computed Maximum Stresses In SHFS Lower Longeron

(Ultimate Static Loads)

Load Case	Max. Tension (ksi)	Max. Compression (ksi)	Max. Shear (ksi)
1	--	98.2	1.10
2	78.5	--	0.88
3	5.3	11.6	0.30
4	0.3	0.5	0.01
5	1.1	2.8	0.11
6	2.9	1.2	0.16
7	2.6	9.7	0.71
8	--	98.3	1.11
9	78.4	--	0.88
10	--	93.8	1.04
11	--	98.6	1.12
12	82.9	--	1.03
13	78.1	--	0.87
14	--	98.8	1.15
15	--	95.6	1.04
16	--	100.9	1.82
17	78.0	--	0.85
18	81.2	--	0.97
19	76.0	--	0.99

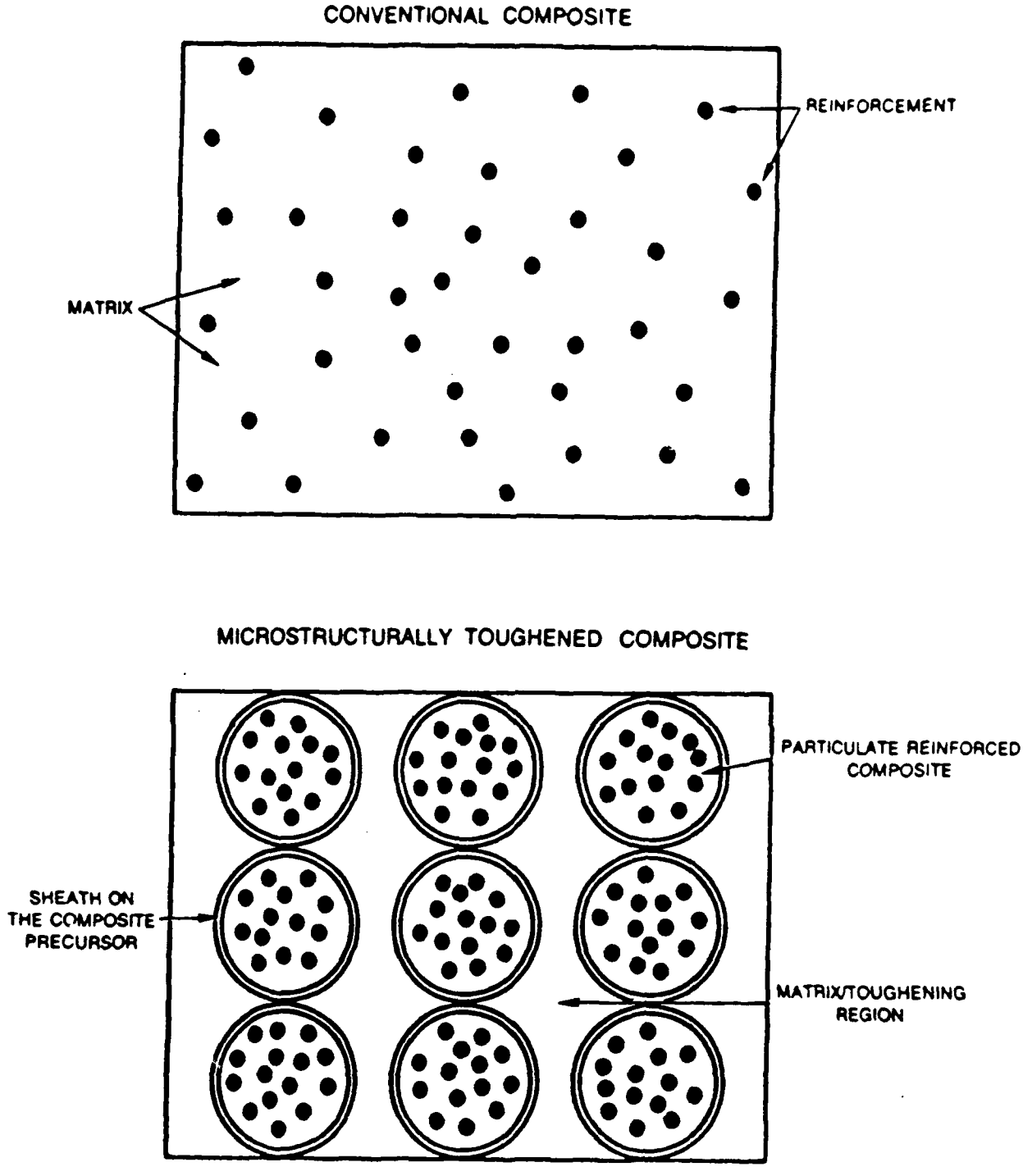

Figure 1. Schematic Comparison Between Conventional and Microstructurally Toughened Particulate Reinforced Composites

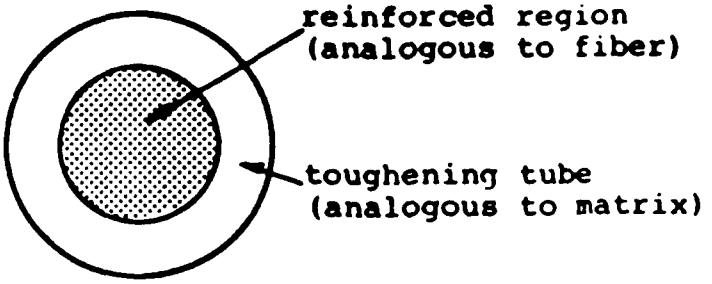

(a) Stress-Strain Constitutive Model

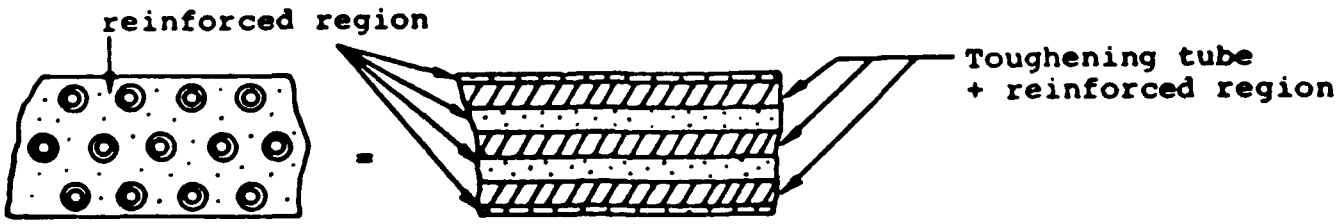

(b) Idealization Of MT Composites With
Dilute Concentration Of Toughening Tubes

Figure 2. Micromechanical Models

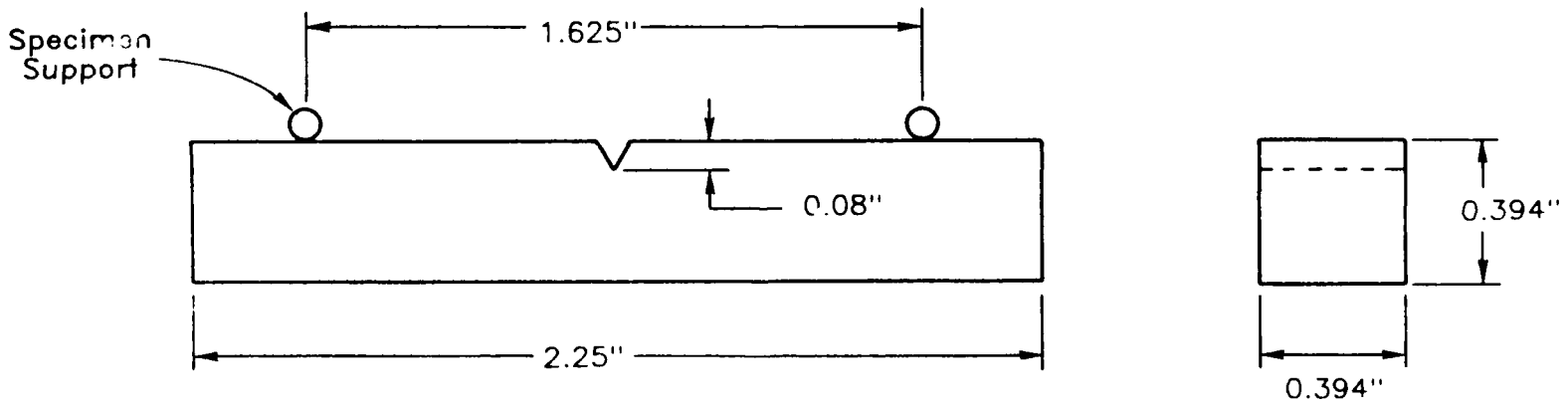

Figure 3. Specimen Used for the Notched Charpy Impact Testing of the MT Composites.

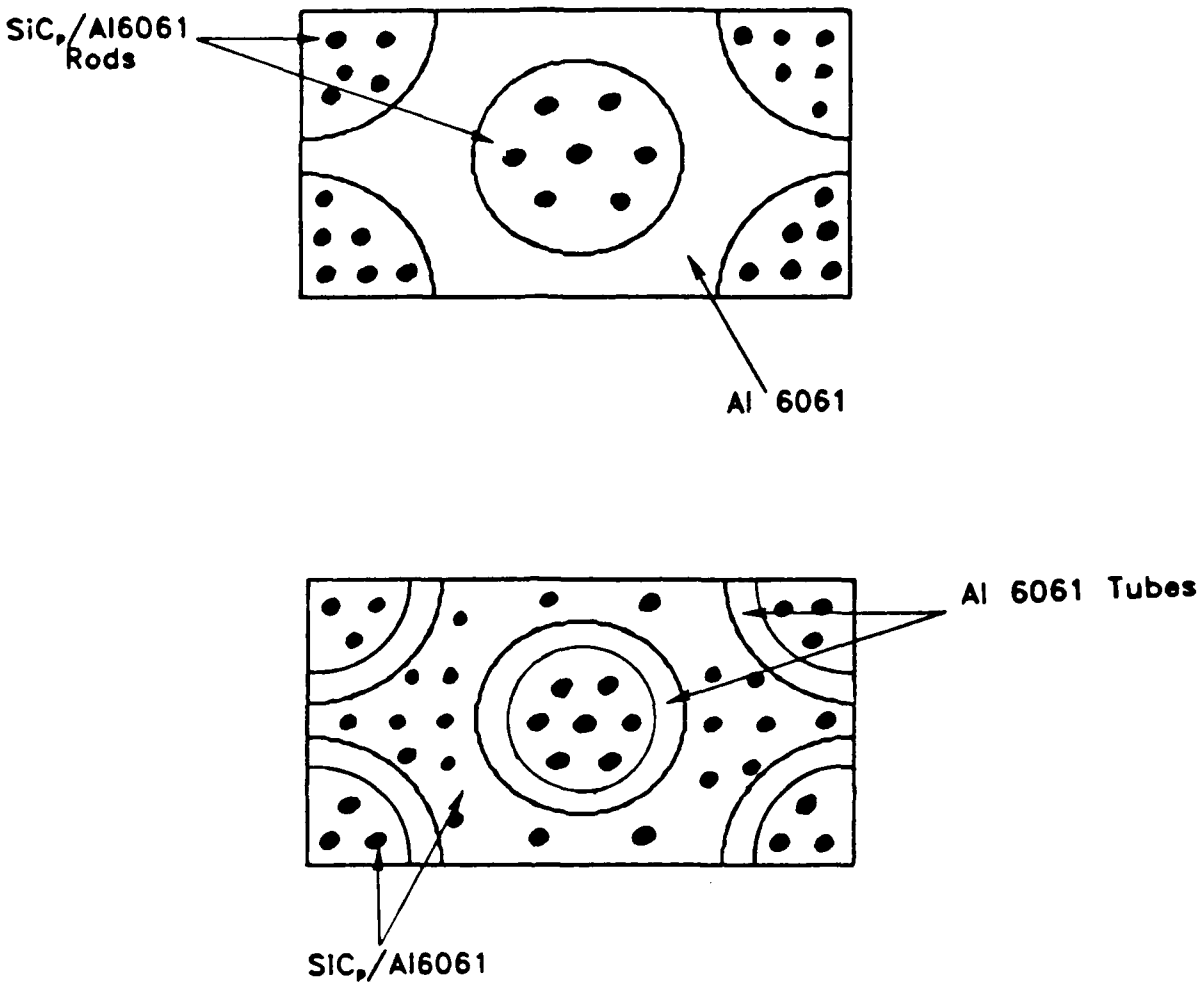

Figure 4. MT Composites Studied In Phase I Program

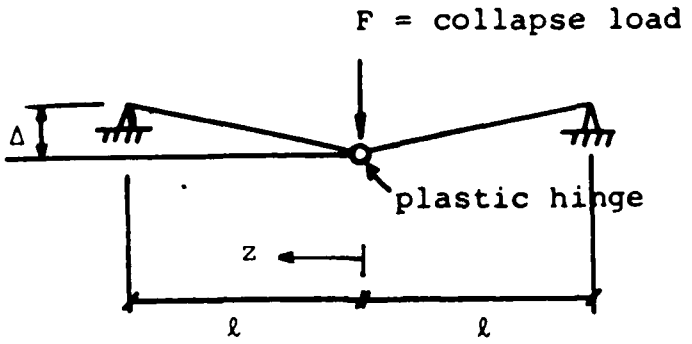

(a) Beam Under Plastic Collapse Load

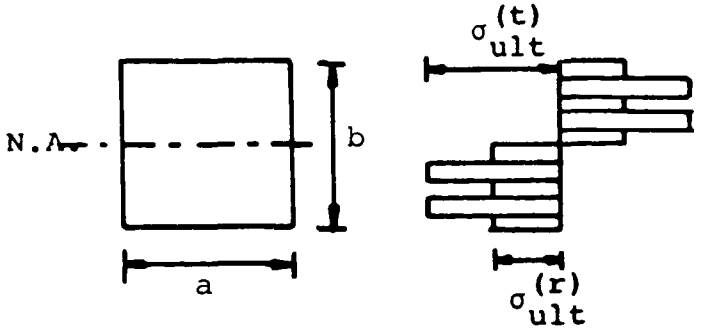

(b) Fully Plastic Stress Distribution On The Cross-Sectional Area Of The Beam

Figure 5. A Simply Supported Beam Under Plastic Collapse Load

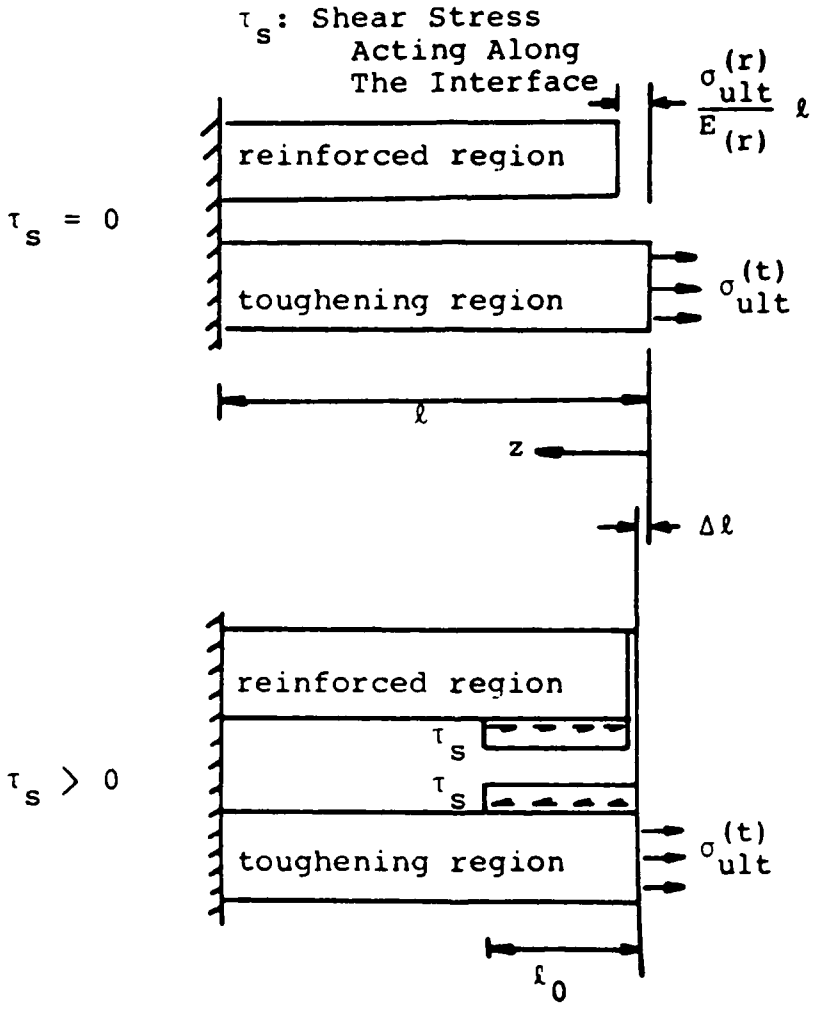

Figure 6. Interaction Between Reinforced And Toughening Regions During Impact Damage

$$C = \frac{\text{Perimeter of the Interface Boundary}}{\text{Cross-Sectional Area of the Toughening Region}}$$

-- Reinforced Region

-- Toughening Region

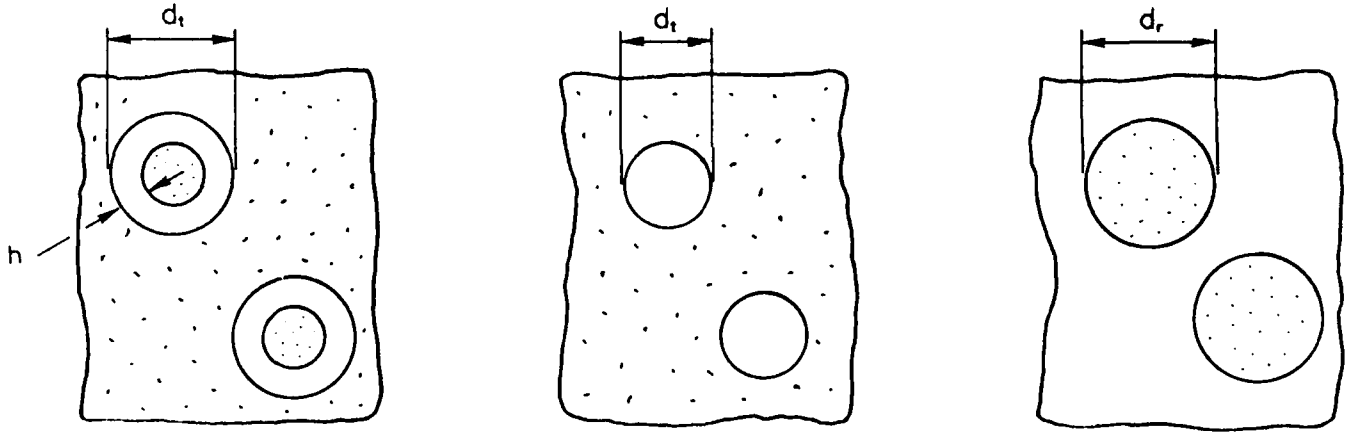

$$C = \frac{2\pi d_t}{\pi d_t h} = \frac{2}{h}$$

$$C = \frac{4}{d_t}$$

$$C = \frac{4}{d_r}\frac{V_r}{V_t}$$

(a) (b) (c)

Figure 7. The Geometric Parameter C for Particulate Reinforced Material Toughened by (a) Tubes, (b) Solid Rods, and (c) Continuous Region.

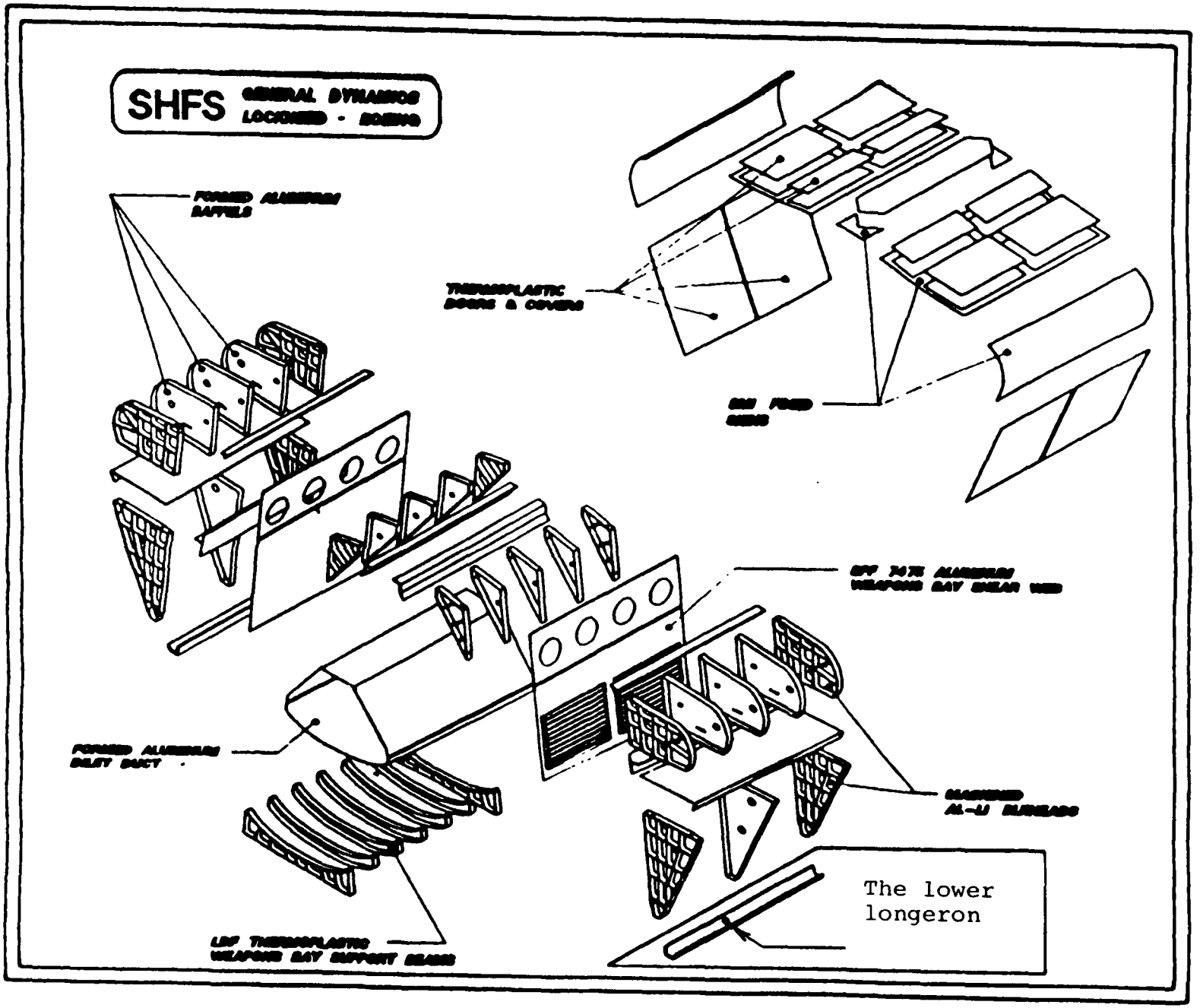

Figure 8. Location of SHFS Lower Longeron

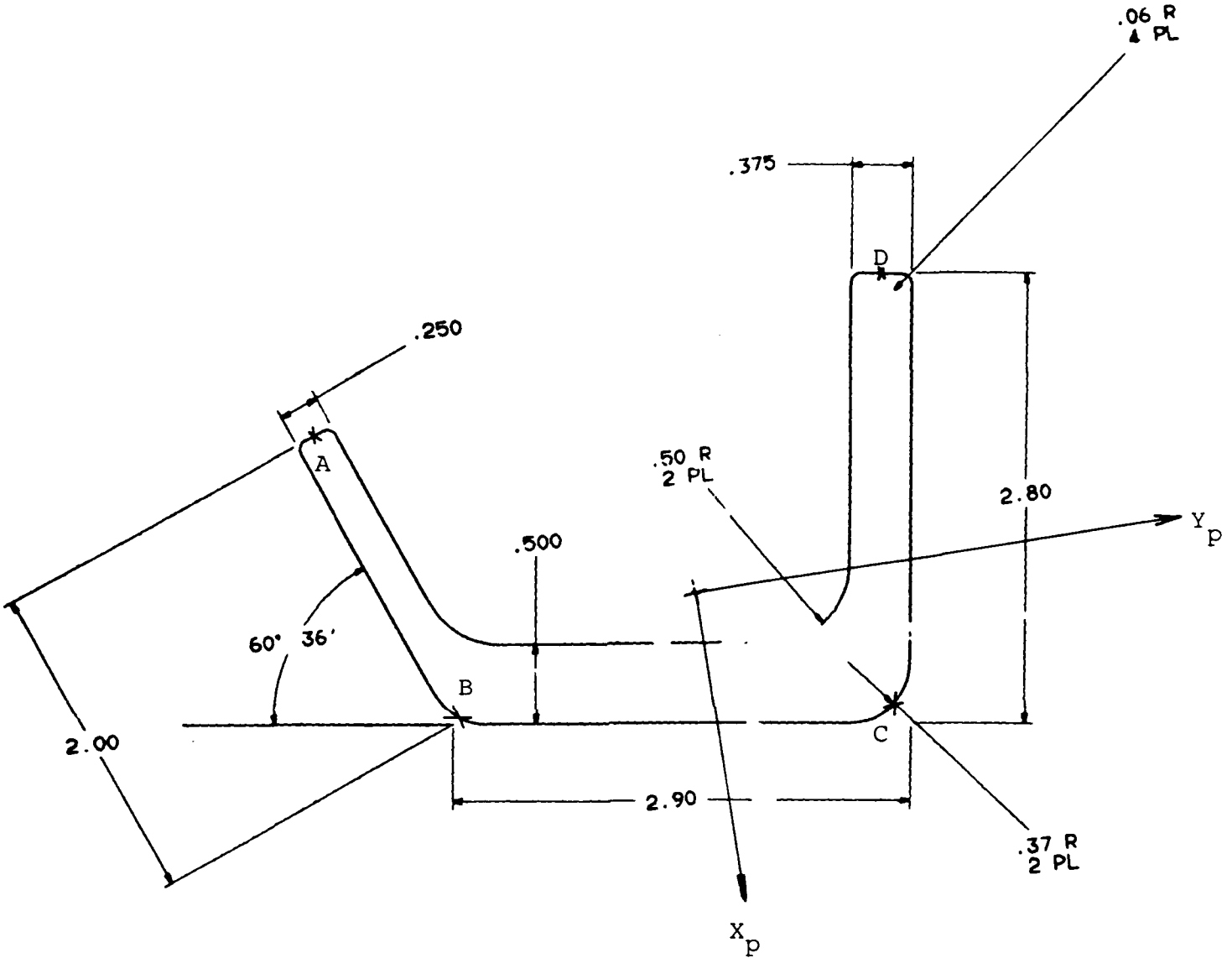

Point	X_p(in)	Y_p(in)
A	-1.34	-2.19
B	0.50	-1.61
C	0.88	1.13
D	-1.75	1.47

Area = 2.78190 in^4

I_{xp} = 4.16682 in^4

I_{yp} = 1.37440 in^4

Figure 9. Cross-Sectional Configurations Of The Longeron Beam

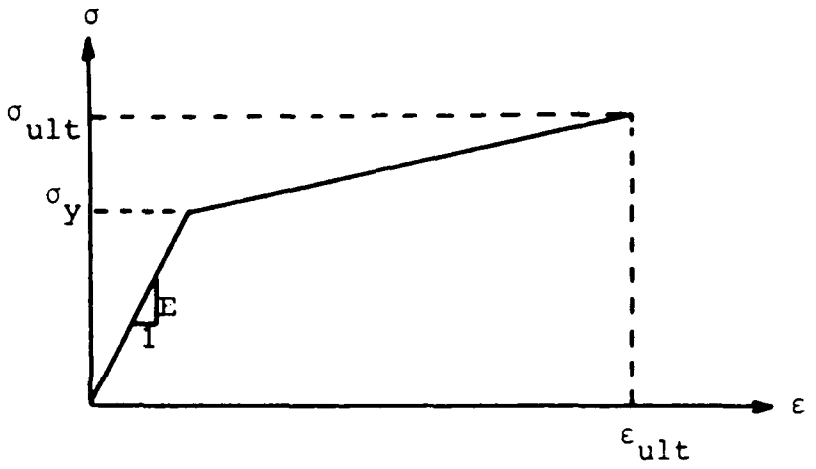

Figure 10. Elastic - Linear Strain Hardening, An Idealized Nonlinear Stress-Strain Curve

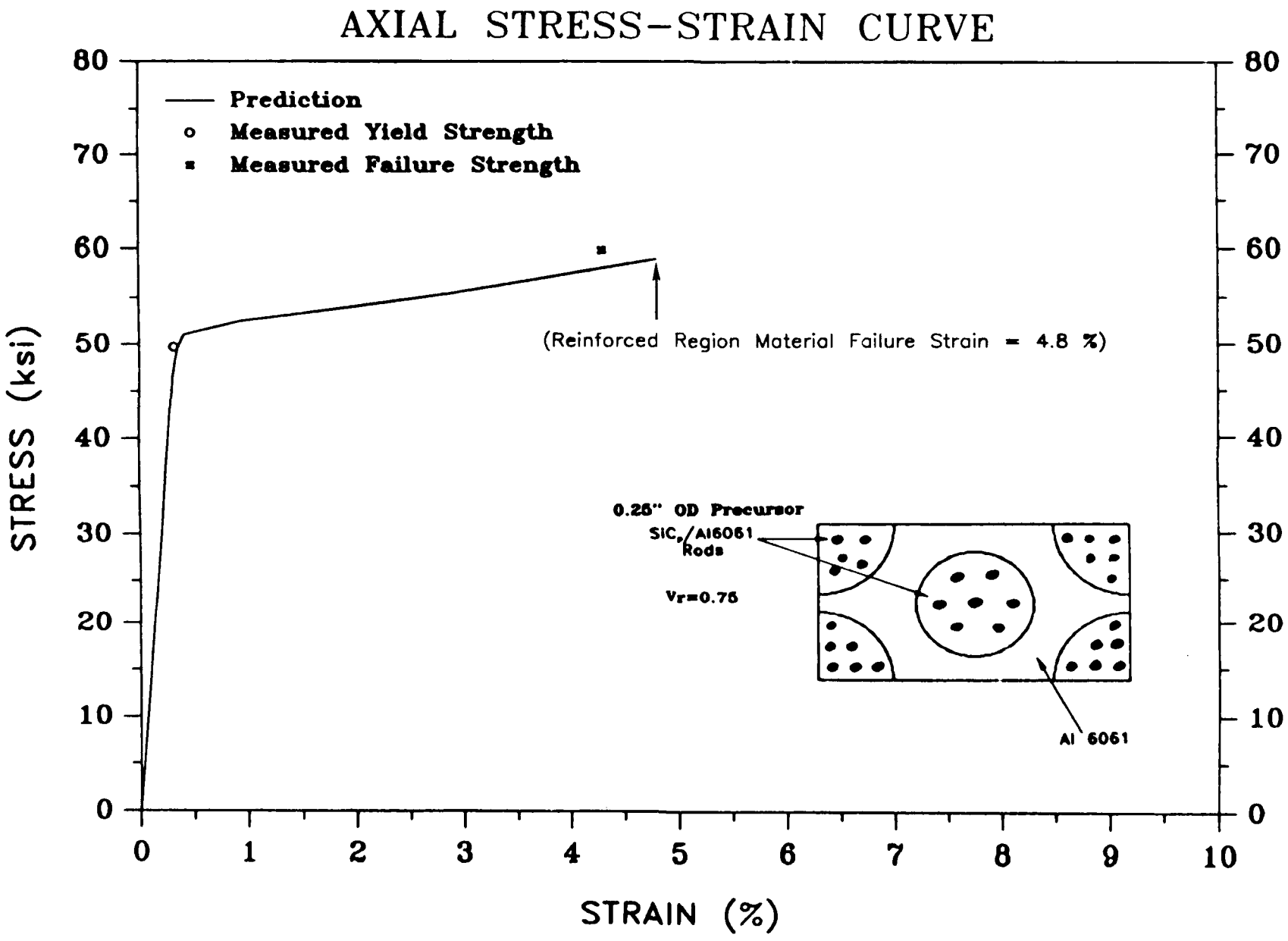

Figure 11. Axial Stress-Strain Curve Of The No. 2 MT Composite

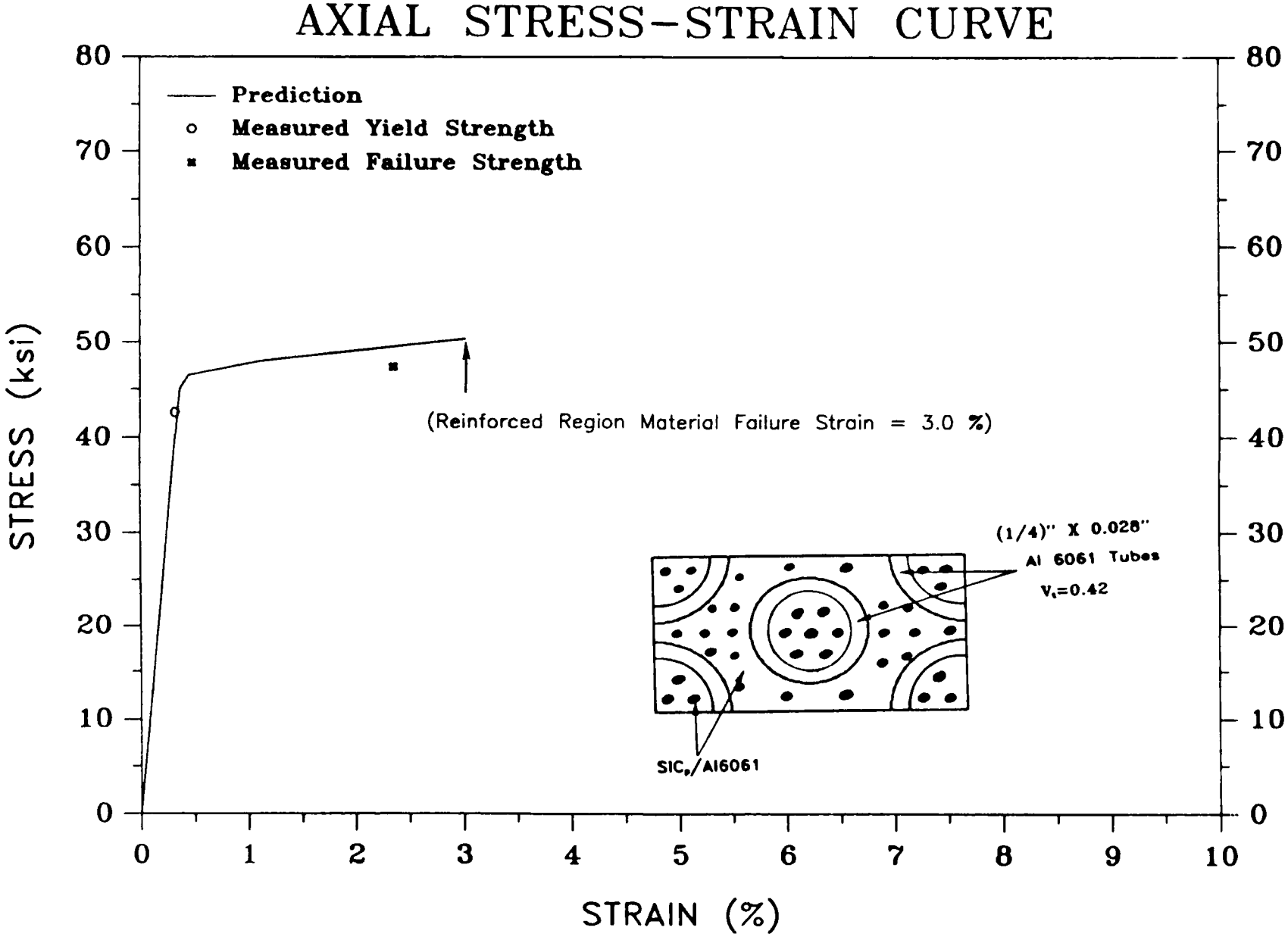

Figure 12. Axial Stress-Strain Curve Of The No. 4 MT Composite

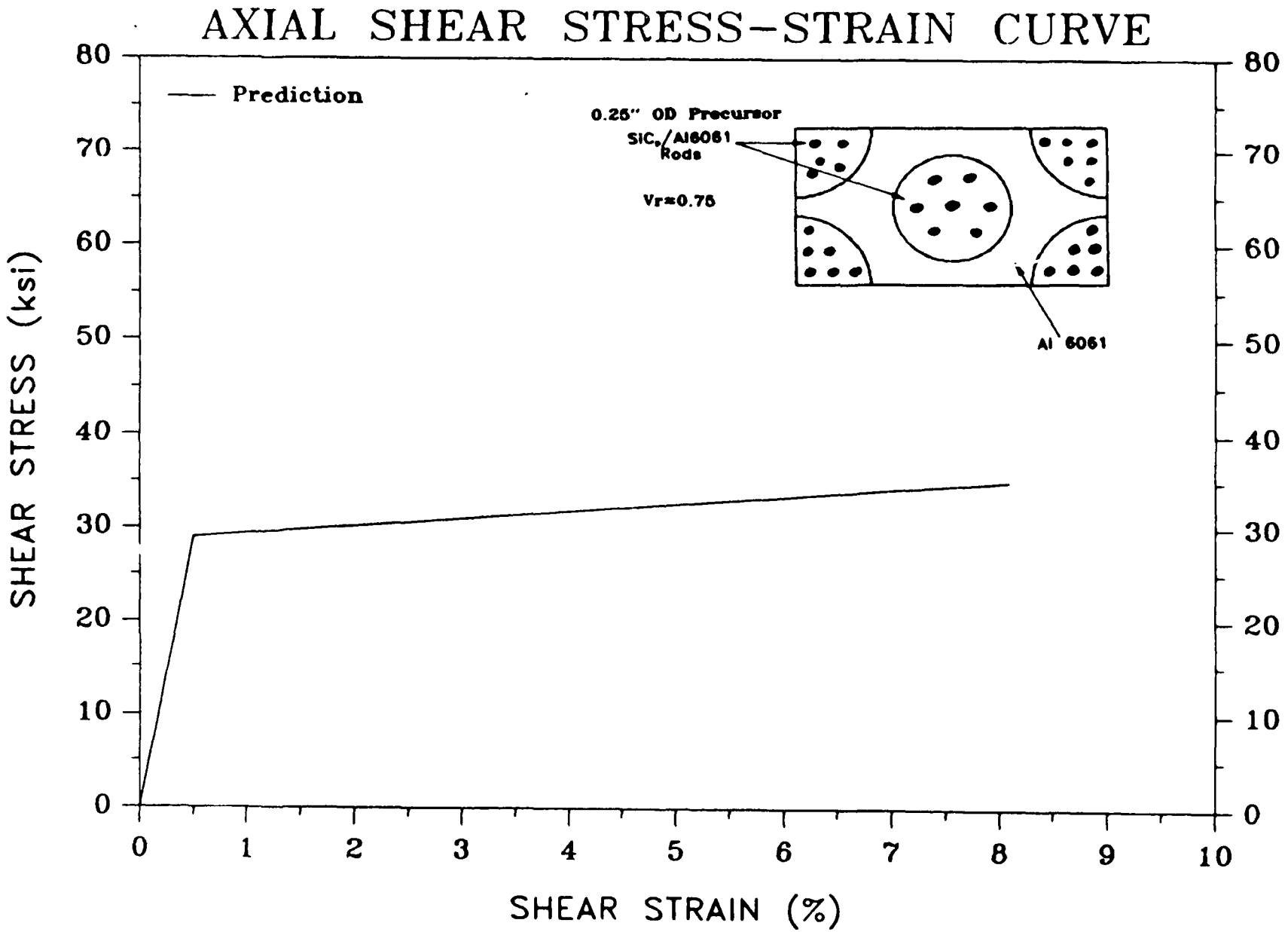

Figure 13. Axial Shear Stress-Strain Curve Of The No. 2 MT Composite

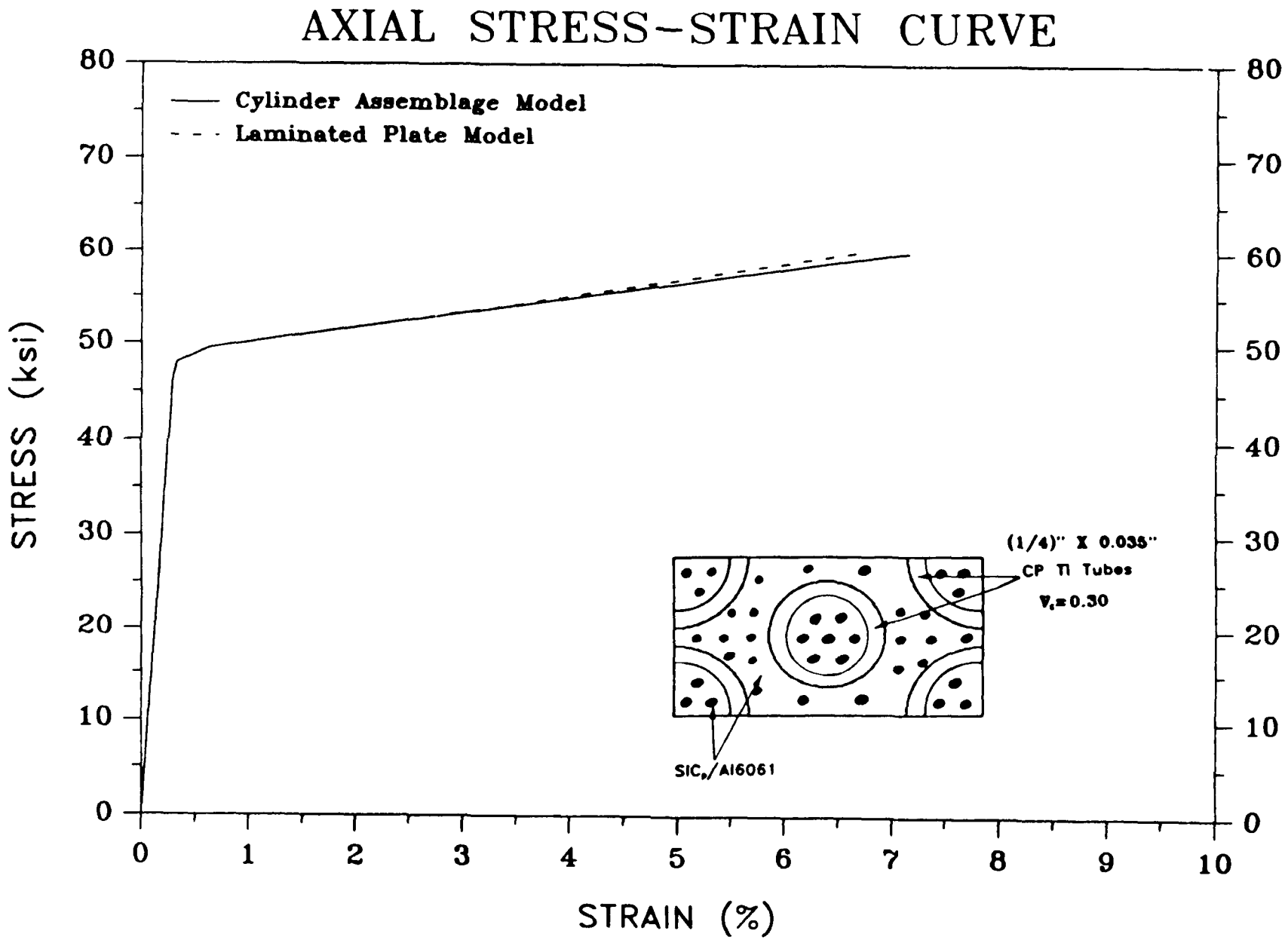

Figure 14. Axial Stress-Strain Curve Of A MT Composite With Low Concentration Of Toughening Tubes

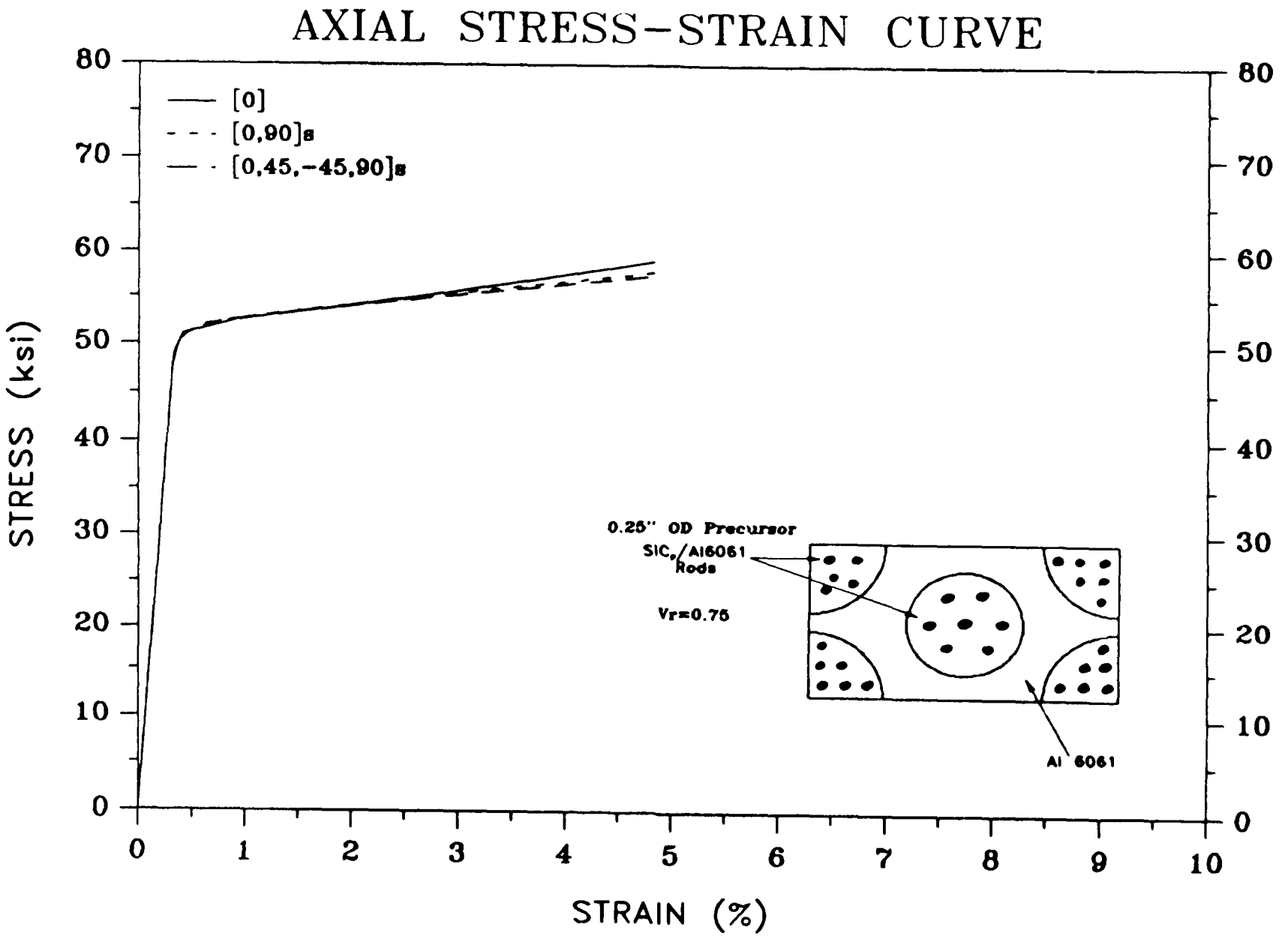

Figure 15. Axial Stress-Strain Curve Of Laminated No. 2 MT Composite

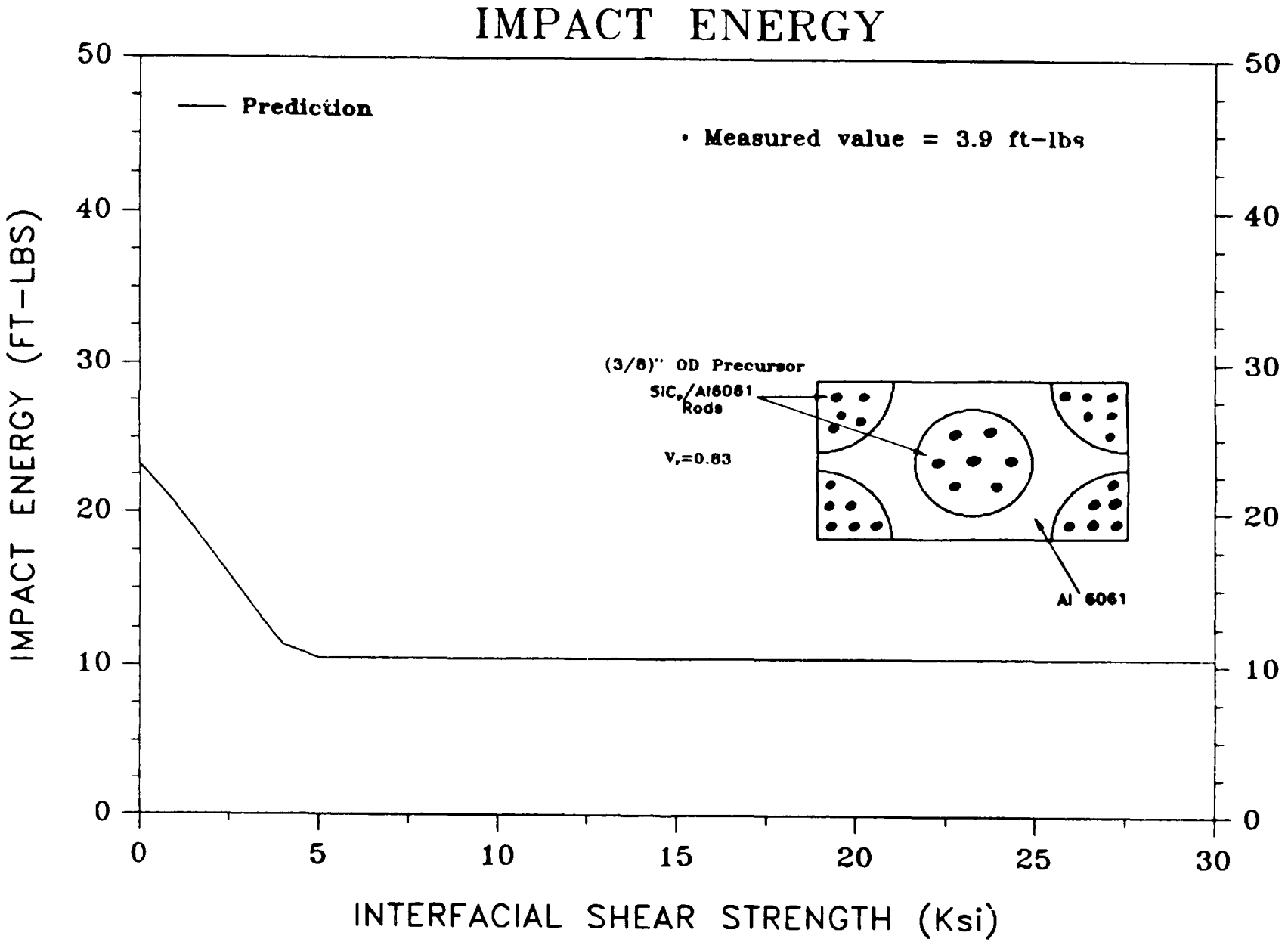

Figure 16. Impact Energy Absorption Capability Of The No. 1 MT Composite

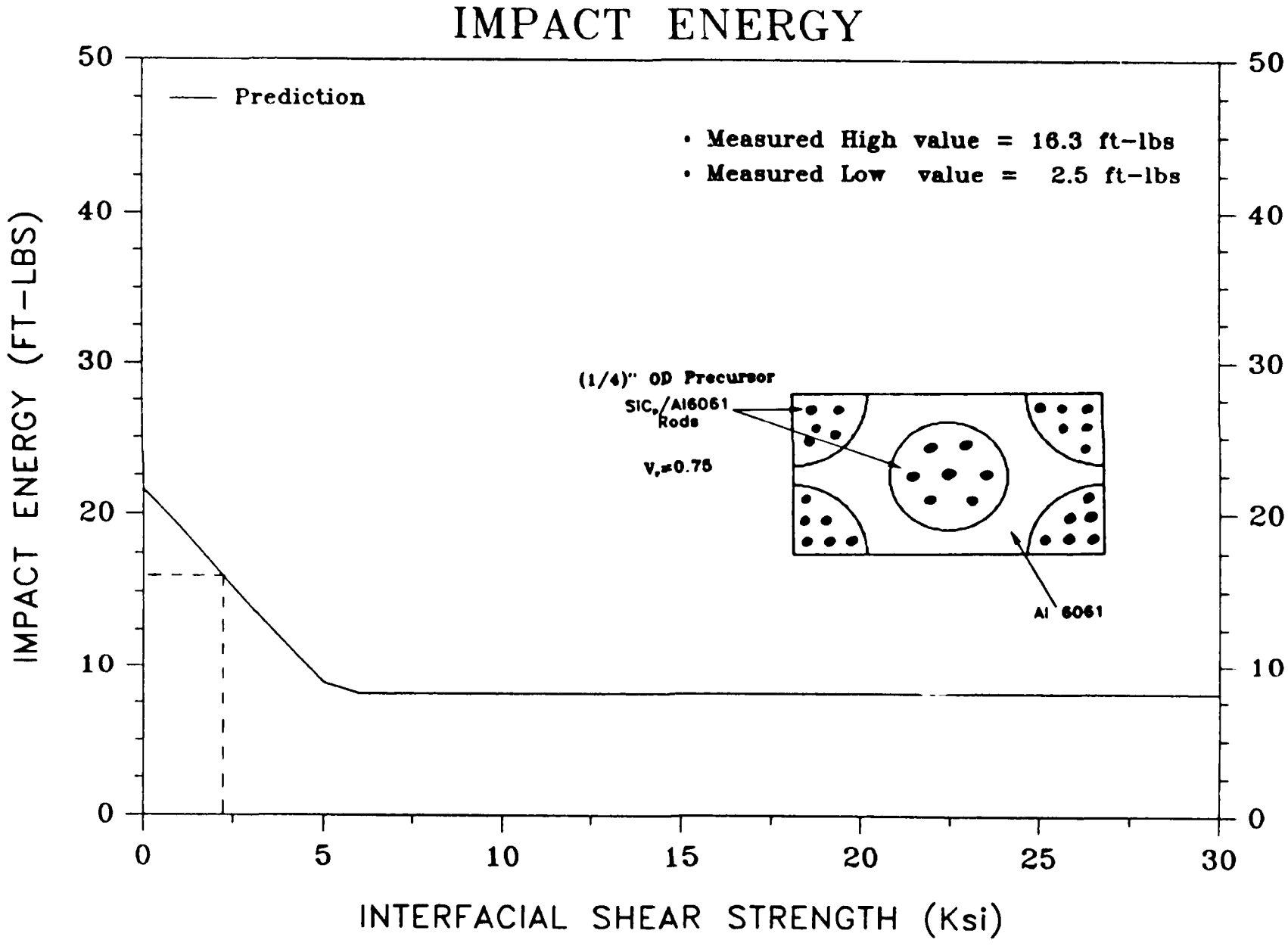

Figure 17. Impact Energy Absorption Capability Of The No. 2 MT Composite

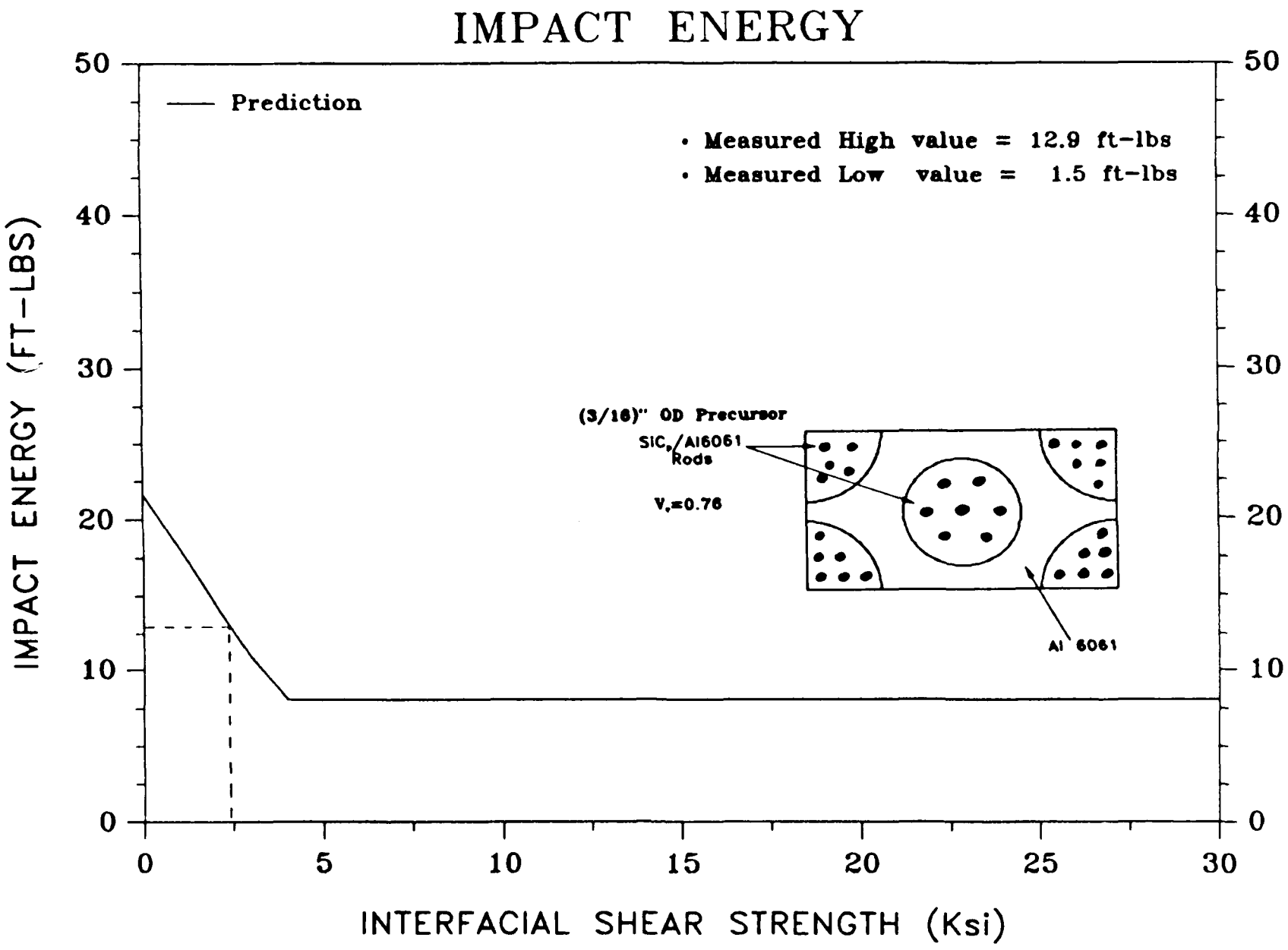

Figure 18. Impact Energy Absorption Capability Of The No. 3 MT Composite

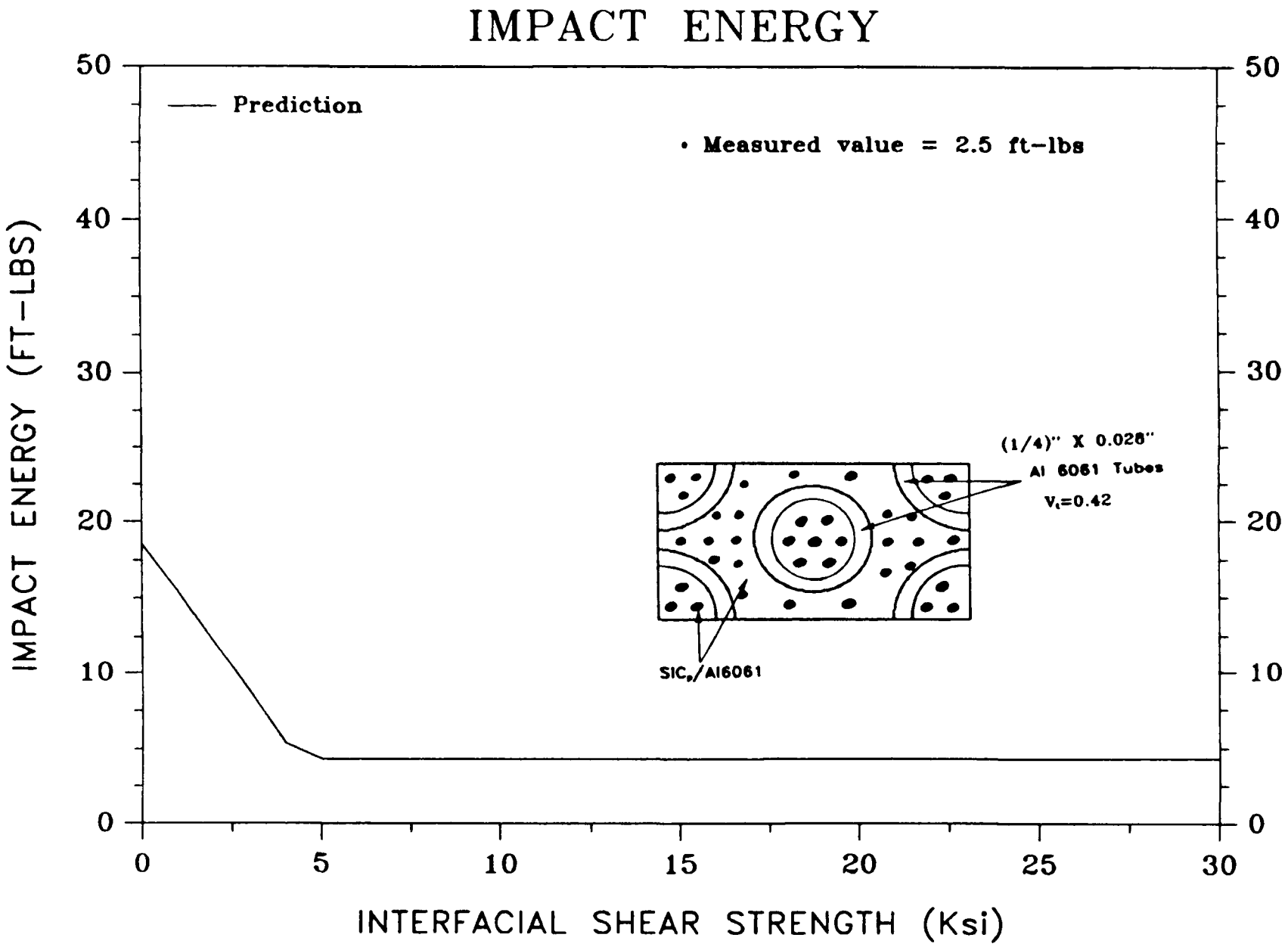

Figure 19. Impact Energy Absorption Capability Of The No. 4 MT Composite

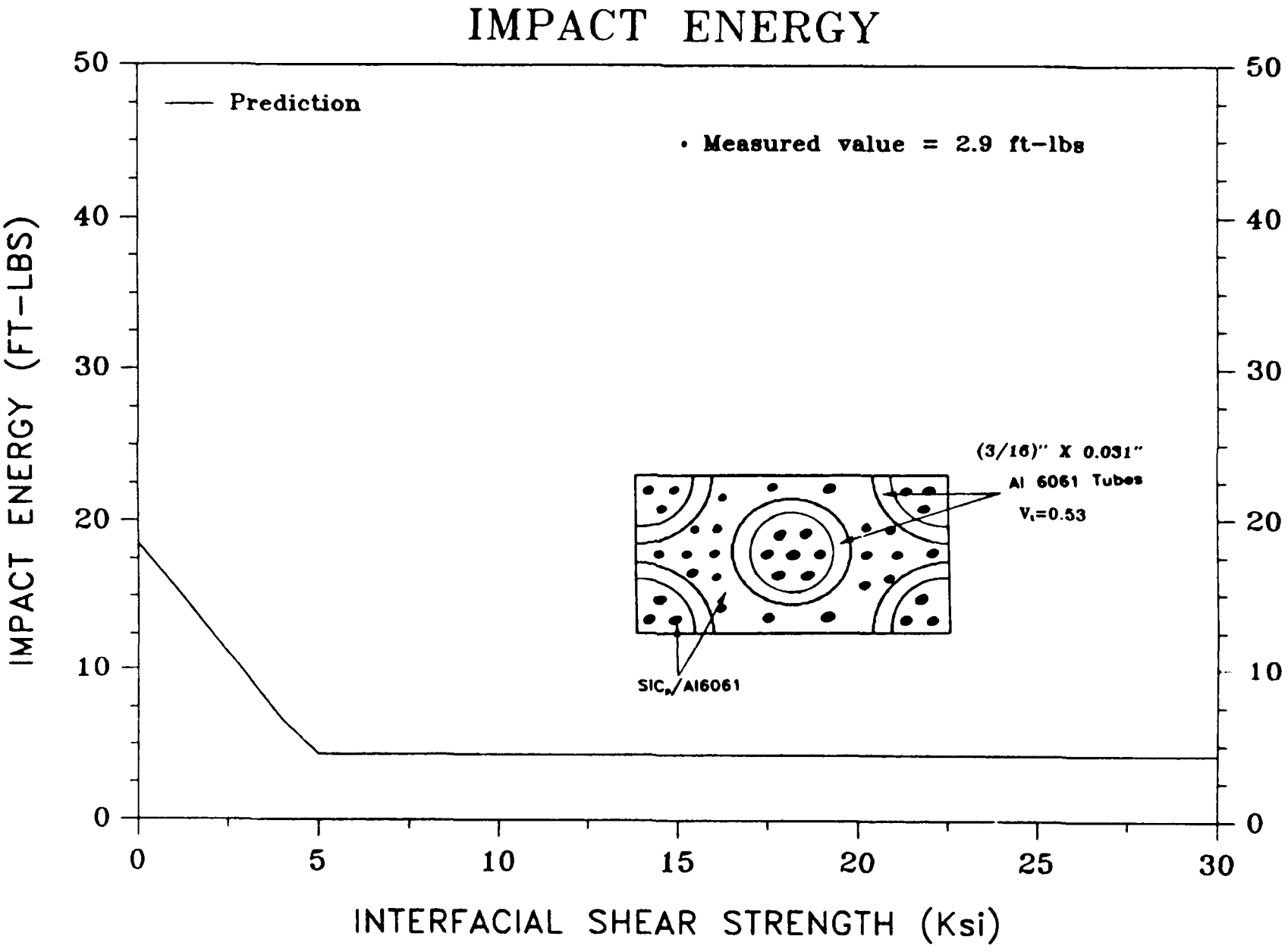

Figure 20. Impact Energy Absorption Capability Of The No. 5 MT Composite

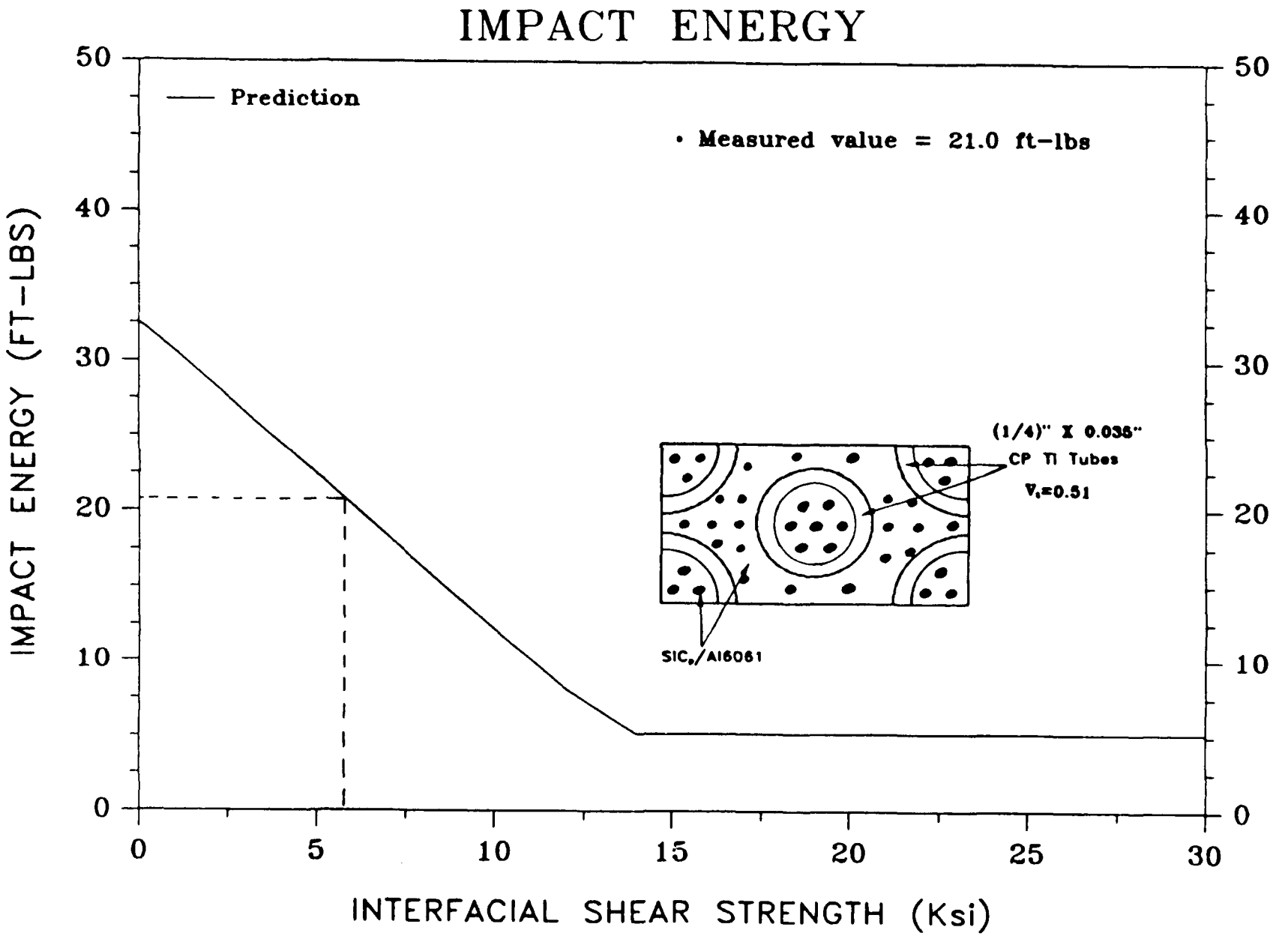

Figure 21. Impact Energy Absorption Capability Of The No. 6 MT Composite

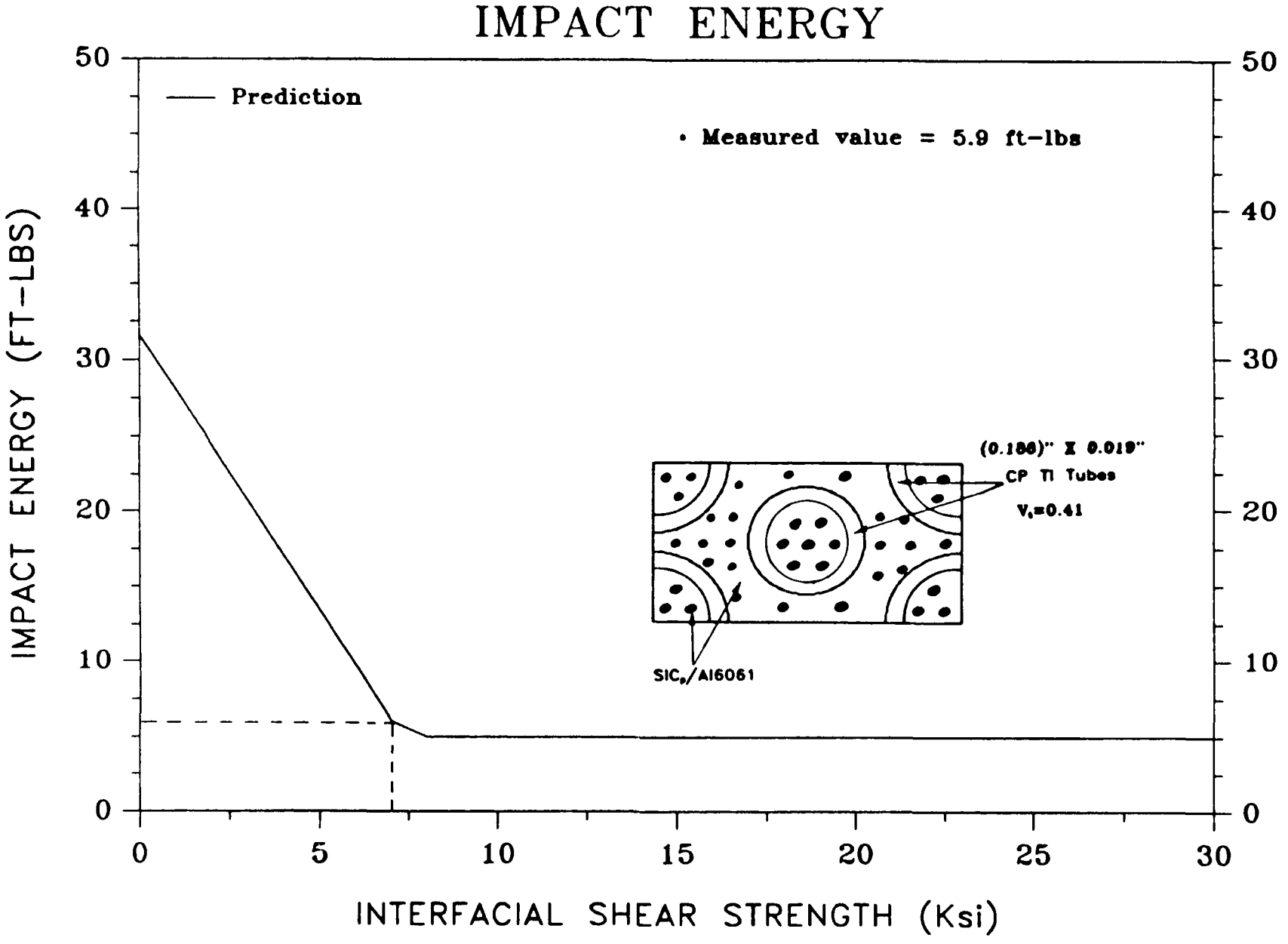

Figure 22. Impact Energy Absorption Capability Of The No. 7 MT Composite

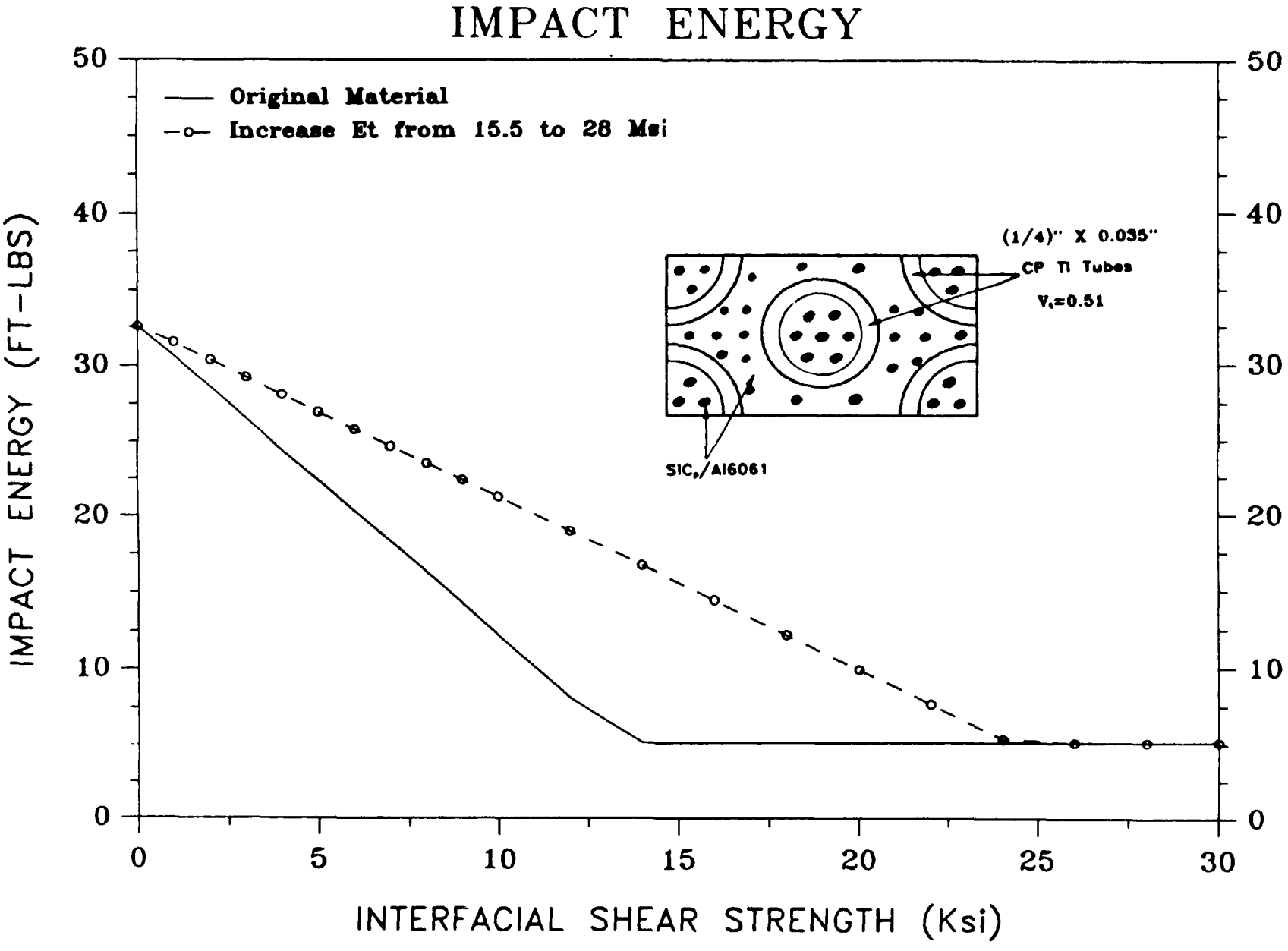

Figure 23. Improve Impact Damage Resistance By Increasing The Stiffness Of The Toughening Region Material

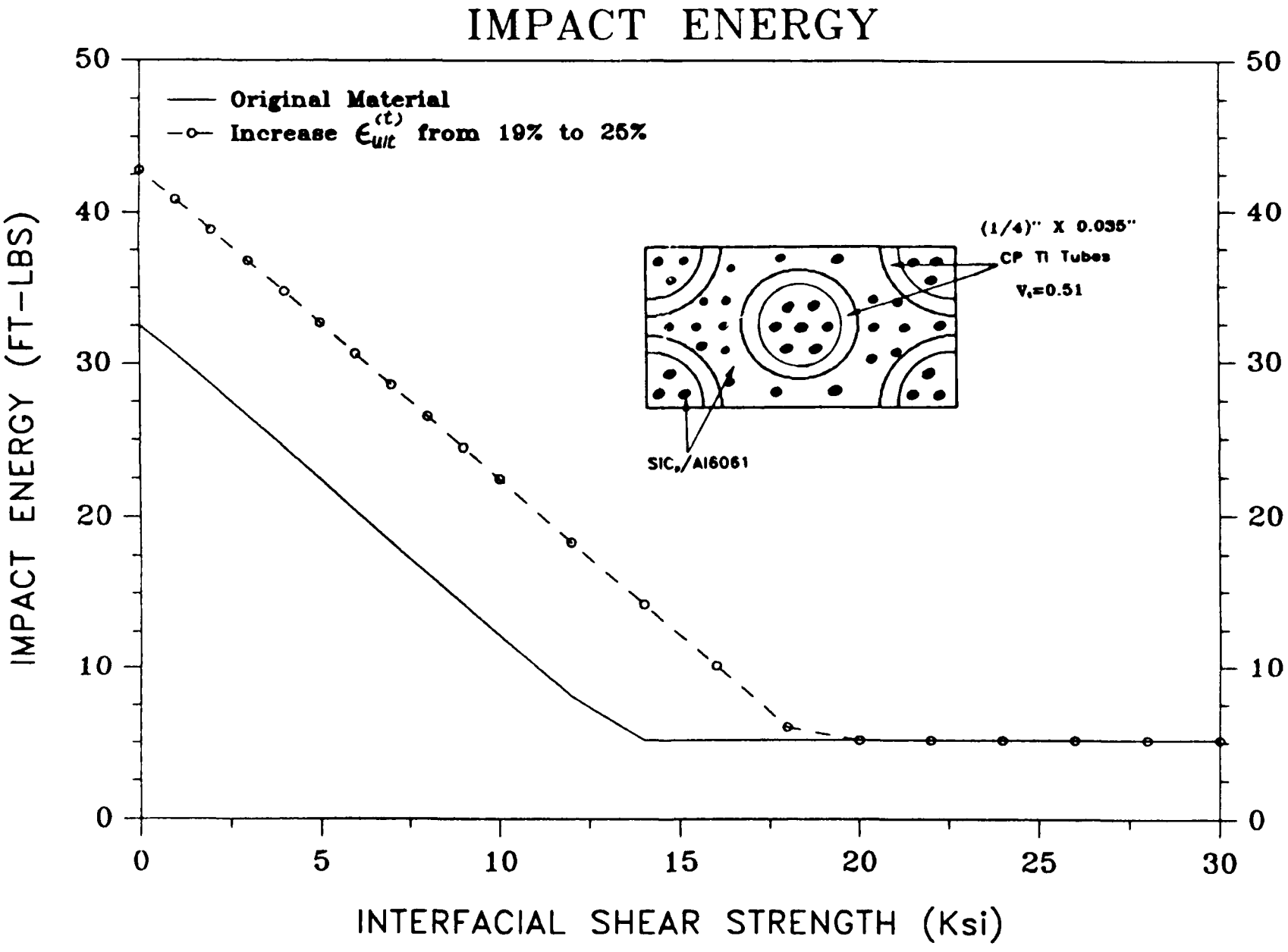

Figure 24. Improve Impact Damage Resistance By Increasing The Failure Strain Of The Toughening Region Material

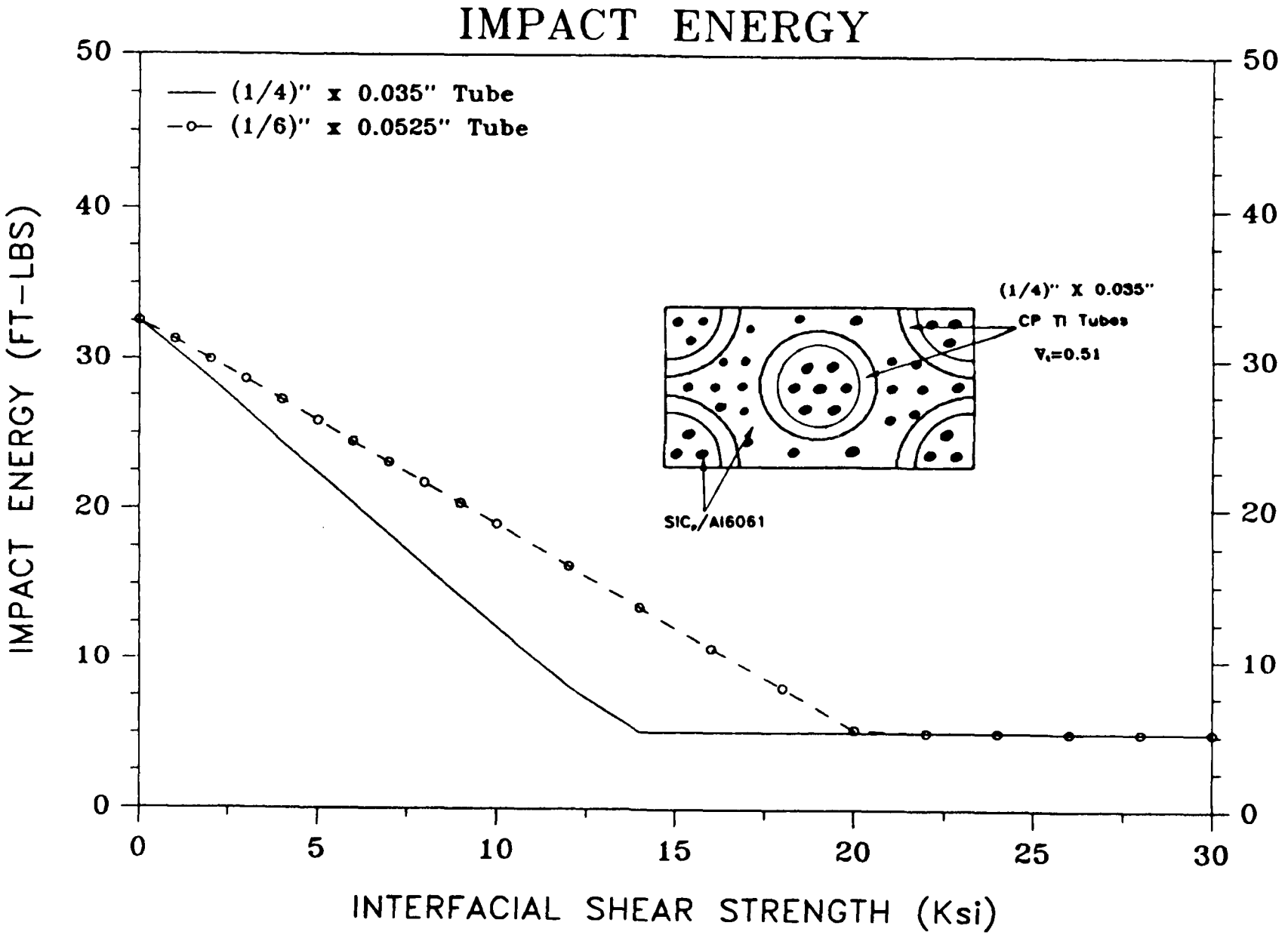

Figure 25. Improve Impact Damage Resistance By Using Thicker Tubes

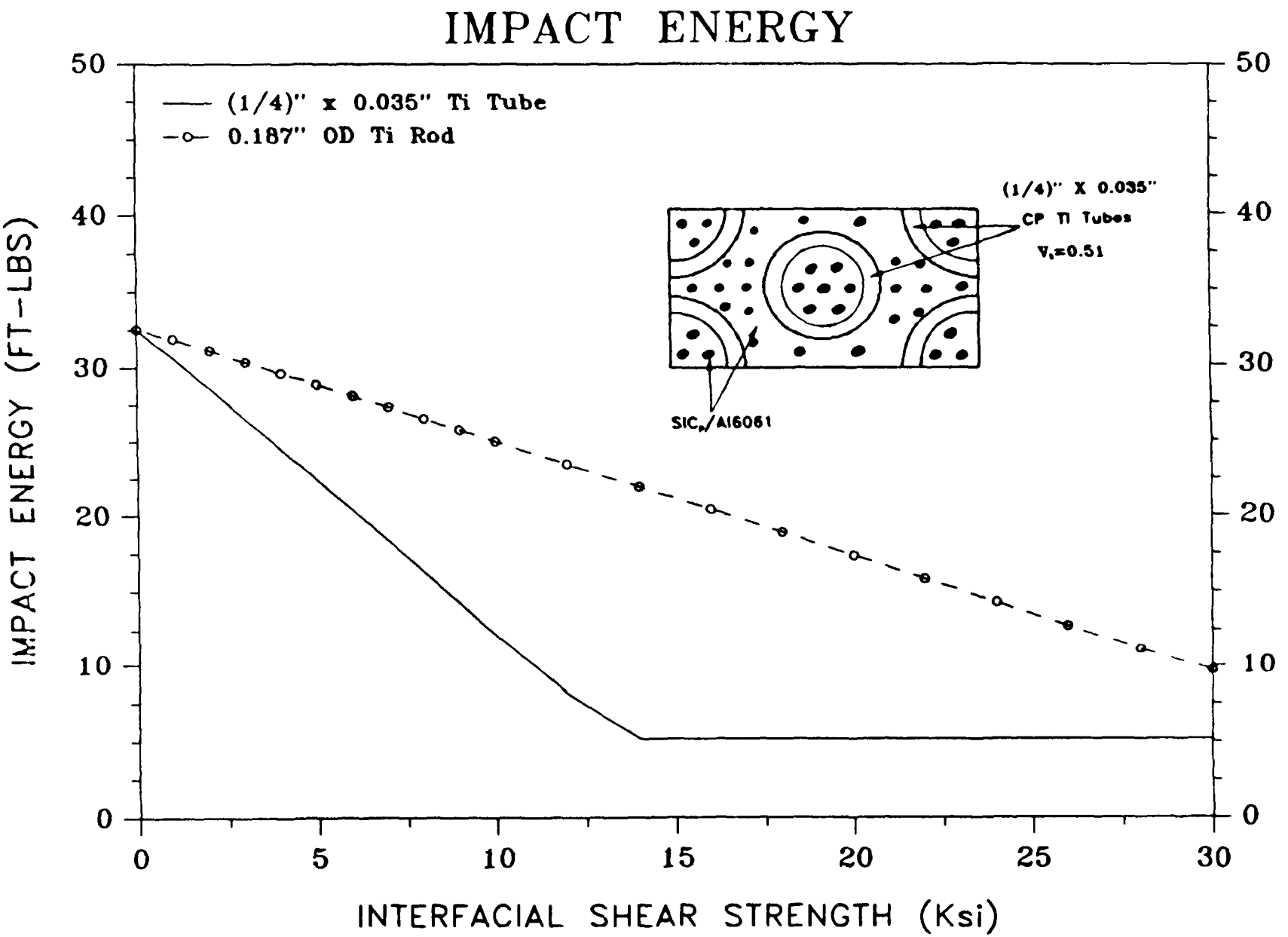

Figure 26. Improve Impact Damage Resistance By Using Solid Rods Instead Of Tubes

APPENDIX

THERMOPLASTIC RESPONSE OF A HOMOGENEOUS SOLID

Assuming a material is elastically isotropic and obeys Mises yield function and Ziegler's kinematic hardening rule during plastic deformation [11], the yield function can be written as

$$f = \frac{1}{2} (s_{ij} - a_{ij})(s_{ij} - a_{ij}) - \kappa^2 (T) = 0 \qquad \text{(A-1)}$$

where

s_{ij}, a_{ij} = the deviatoric components of σ_{ij} and α_{ij}, respectively;

σ_{ij} = current stress state;

α_{ij} = current center of yield surface in stress space;

$\kappa(T)$ = yield stress in simple shear, and is assumed to be a function of temperature T.

Ziegler's kinematic hardening rule specifies the kinematic motion of the yield surface during plastic deformation as

$$\dot{\alpha}_{ij} = \dot{\mu} (\sigma_{ij} - \alpha_{ij}), \qquad \text{(A-2a)}$$

or, in the deviatoric stress space,

$$\dot{a}_{ij} = \dot{\mu} (s_{ij} - a_{ij}), \qquad \text{(A-2b)}$$

where $\dot{\mu}$ is to be determined later.

The yield function, equation (A-1), remains equal to zero during plastic deformation. Therefore, the following consistency equation has to be satisfied whenever plastic deformation takes place,

$$\dot{f} = (\partial f/\partial s_{ij})\dot{s}_{ij} + (\partial f/\partial a_{ij})\dot{a}_{ij} + (\partial f/\partial \kappa)\dot{\kappa}$$

$$= (s_{ij} - a_{ij})(\dot{s}_{ij} - \dot{a}_{ij}) - 2\kappa\dot{\kappa} = 0. \tag{A-3}$$

Substituting equation (A-2b) for the $\dot{a}_{ij}$ in equation (A-3) and solving for $\dot{\mu}$, one obtains

$$\dot{\mu} = [(s_{ij} - a_{ij})\dot{s}_{ij} - 2\kappa\dot{\kappa}]/(2\kappa^2). \tag{A-4}$$

Note that the relation $(s_{ij} - a_{ij})(s_{ij} - a_{ij}) = 2\kappa^2$, i.e., equation (A-1), has also been utilized to obtain (A-4).

The plastic strain increment, from the normality rule, is

$$\dot{\epsilon}^p_{ij} = \dot{\lambda}(\partial f/\partial s_{ij}) = \dot{\lambda}(s_{ij} - a_{ij}). \tag{A-5}$$

To determine $\dot{\lambda}$, we follow Ziegler's assumption that the projection of plastic strain increment on the exterior normal vector of the yield surface and the projection of $\dot{a}_{ij}$ on the same normal vector differ only by a constant c, i.e.,

$$c(\partial f/\partial s_{ij})\dot{\epsilon}^p_{ij} = (\partial f/\partial s_{ij})\dot{a}_{ij}. \tag{A-6}$$

Carrying out the differentiations and making use of the consistency equation (A-3), equation (A-6) becomes

$$c(s_{ij} - a_{ij})\dot{\epsilon}^p_{ij} = (s_{ij} - a_{ij})\dot{s}_{ij} - 2\kappa\dot{\kappa}. \tag{A-7}$$

For the case of simple tension in x_1 direction, (A-7) takes the form

$$\dot{\epsilon}^p_{11} = \frac{2}{3c}(\dot{\sigma}_{11} - \sqrt{3}\,\dot{\kappa}). \tag{A-8}$$

The magnitude of c can now be evaluated by comparing (A-8) with the known incremental stress-plastic strain relation in simple tension, i.e.,

$$\dot{\epsilon}^p_{11} = \frac{1}{H}(\dot{\sigma}_{11} - \sqrt{3}\,\dot{\kappa}). \tag{A-9}$$

where H is the instantaneous hardening parameter. Thus, one has

$$c = 2H / 3. \tag{A-10}$$

Now, $\dot{\lambda}$ can be solved by substituting (A-5) and (A-10) into (A-7). The result is

$$\dot{\lambda} = \frac{3}{4H\kappa^2} [(s_{k\ell} - a_{k\ell})\dot{s}_{k\ell} - 2\kappa\dot{\kappa}]. \tag{A-11}$$

Accordingly, the plastic strain increment follows from (A-5), with $\dot{\lambda}$ taken from (A-11),

$$\dot{\epsilon}^p_{ij} = \frac{3}{4H\kappa^2} [(s_{k\ell} - a_{k\ell})\dot{s}_{k\ell} - 2\kappa\dot{\kappa}](s_{ij} - a_{ij}). \tag{A-12}$$

Equation (A-12) can be written in a matrix form comparable to equation (7),

$$\underset{\sim}{\dot{\epsilon}}^p = \underset{\sim}{M}^p \, \underset{\sim}{\dot{\sigma}} + \underset{\sim}{\dot{\epsilon}}^{pT}. \tag{7}$$

The instantaneous compliances $\underset{\sim}{M}^p$ and $\underset{\sim}{\dot{\epsilon}}^{pT}$ can now be identified as

$$\underset{\sim}{M}^p = \frac{3}{4H\kappa^2} \begin{bmatrix} (s_1^*)^2 & s_1^* s_2^* & 2s_1^* s_3^* & s_1^* s_4^* & 2s_1^* s_5^* & 2s_1^* s_6^* \\ & (s_2^*)^2 & 2s_2^* s_3^* & s_2^* s_4^* & 2s_2^* s_5^* & 2s_2^* s_6^* \\ & & 4(s_3^*)^2 & 2s_3^* s_4^* & 4s_3^* s_5^* & 4s_3^* s_6^* \\ & & & (s_4^*)^2 & 2s_4^* s_5^* & 2s_4^* s_6^* \\ & & & & 4(s_5^*)^2 & 4s_5^* s_6^* \\ \text{Symm.} & & & & & 4(s_6^*)^2 \end{bmatrix} \tag{A-13}$$

$$\underset{\sim}{\epsilon}^{pT} = - \frac{3\dot{\kappa}}{2H\kappa} [s_1^* \quad s_2^* \quad 2s_3^* \quad s_4^* \quad 2s_5^* \quad 2s_6^*] \tag{A-14}$$

where

$$[s_1^* \quad s_2^* \quad s_3^* \quad s_4^* \quad s_5^* \quad s_6^*]$$

$$= [s_{11}^* \quad s_{22}^* \quad s_{12}^* \quad s_{33}^* \quad s_{13}^* \quad s_{23}^*],$$

and

$$s_{ij}^* = s_{ij} - a_{ij}. \tag{A-15}$$